

Superconducting Coupler with Exponentially Large On:Off Ratio

Catherine Leroux,^{1,*} Agustin Di Paolo^{1,†} and Alexandre Blais^{1,2}

¹*Institut quantique & Département de Physique, Université de Sherbrooke, Sherbrooke, Québec J1K 2R1, Canada*

²*Canadian Institute for Advanced Research, Toronto, Ontario, Canada*

 (Received 7 September 2021; revised 22 September 2021; accepted 11 November 2021; published 27 December 2021)

Tunable two-qubit couplers offer an avenue to mitigate errors in multiqubit superconducting quantum processors. However, most couplers achieve this by fine tuning circuit parameters and often target specific couplings, such as the spurious ZZ interaction. We introduce a superconducting coupler that alleviates these limitations by suppressing all two-qubit interactions with an exponentially large on:off ratio and without the need for fine tuning. Our approach is based on a bus mode supplemented by an ancillary nonlinear resonator mode. Driving the ancillary mode leads to a coupler-state-dependent field displacement in the resonator that, in turn, results in an exponential suppression of real and virtual two-qubit interactions with respect to the drive power. A superconducting circuit implementation supporting the proposed mechanism is presented.

DOI: [10.1103/PhysRevApplied.16.064062](https://doi.org/10.1103/PhysRevApplied.16.064062)

I. INTRODUCTION

Two-qubit couplers are useful components for quantum information processing as they enable fast and high-fidelity operations between qubits while reducing crosstalk during idle times. Several superconducting coupler designs have been theoretically proposed and experimentally implemented [1–18]. These devices can, in principle, offer precise control of two-qubit interactions while helping to mitigate frequency crowding effects in multiqubit processors such as to improve gate speed and fidelity. There are, however, limitations to the performance of current couplers. For instance, while couplers are designed to activate interactions between qubits on-demand, spurious interactions can remain active when the coupler is tuned to its *off* state. A common example is the ubiquitous always-on cross-Kerr, or ZZ , coupling [3,4,19–22]. A second difficulty is that the coupler's on:off ratio is often sensitive to first order in a control parameter, such as an external magnetic flux, thus requiring fine tuning and frequent calibration. Couplers that do not rely on frequency tuning do not suffer from this, but the lack of tunability comes with its own set of challenges such as large crosstalk errors during idle times. Finally, the impact of these effects could be exacerbated in multiqubit devices where frequency shifts from spectator qubits can counteract fine tuning.

Here, we alleviate these issues by introducing a tunable coupler with an exponentially large on:off ratio and that does not require fine tuning of the coupler or qubit

parameters; see Fig. 1. This is realized by adapting some of the ideas of protected qubits to coupler designs. Broadly speaking, the large on:off ratio is achieved by connecting a bus mode responsible for qubit-qubit interactions to an ancillary driven nonlinear resonator, in such a way that the bus transition matrix elements that control two-qubit interactions vanish exponentially with respect to the amplitude of the drive on the ancillary system. This key feature renders the coupler, which includes the bus and the driven nonlinear resonator modes, exponentially insensitive to noise and relaxes the need for fine tuning. This proposal is particularly well suited to processors based on protected qubits such as Kerr-cat [23,24] and fluxonium [25,26] qubits where exponential suppression of multiqubit crosstalk would enhance the intrinsic robustness of the processor against noise.

This paper is organized as follows. In Sec. II we describe the physical mechanism enabling the exponential suppression of two-qubit interactions and introduce a model Hamiltonian realizing this mechanism. In Sec. III, we report numerical results demonstrating the exponential suppression of qubit-qubit interactions mediated by the coupler and discuss implications in the context of large-scale processors as well as some of the limitations of the proposed design. Finally, we introduce a superconducting circuit implementation of these ideas in Sec. V.

II. WORKING PRINCIPLE AND HAMILTONIAN MODEL

Figures 2(a) and 2(b) schematically illustrate the proposed device consisting of two qubits, labeled Q_1 and

*Catherine.Leroux@USherbrooke.ca

†adipaolo@mit.edu

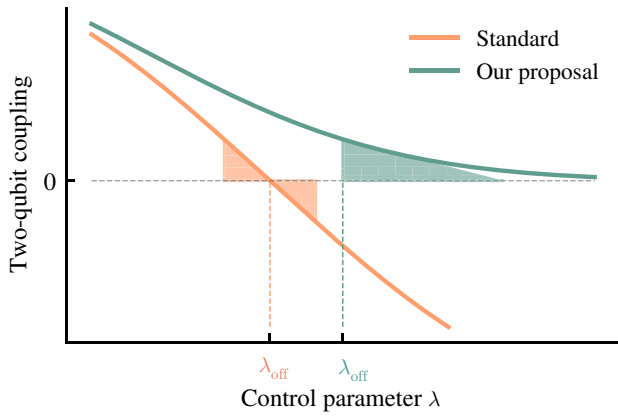


FIG. 1. Two-qubit coupling strength versus control parameter. For standard coupler designs, the on:off ratio depends linearly with respect to a control parameter λ (orange line). This results in linear sensitivity to noise in the control parameter. Our coupler design implements a two-qubit coupling that can be exponentially suppressed with respect to the control parameter (green line). Therefore, sensitivity to noise in the *off* state of the coupler is exponentially small, and the need for fine tuning is relaxed.

Q_2 , which are coupled via a bus mode B also connected to a driven nonlinear resonator mode R . In the absence of a drive on the nonlinear resonator, the system reduces to a standard circuit QED setup where the bus mediates energy-exchange interactions between the qubits [3,4,20–22,27,28]. We assume that the qubit-bus interactions (full lines) can be modeled by a Jaynes-Cummings-type Hamiltonian. On the other hand, the bus-resonator interaction (dashed line) is engineered such that, upon driving R , the resonator field undergoes a bus-state-dependent displacement characteristic of a longitudinal interaction [29–32]. As a result, a distinct resonator coherent state $|\alpha_n\rangle_r$ is associated with each bus eigenstate $|n\rangle_b$, such that the states $|\psi_n\rangle = |n\rangle_b|\alpha_n\rangle_r$ are stabilized. Then, transitions

between the m th and n th low-energy eigenstates of the bus are suppressed in the coherent-state amplitude

$$|n\rangle\langle m|_b \otimes 1_r \rightarrow e^{-|\alpha_n - \alpha_m|^2/2} |\psi_n\rangle\langle\psi_m|. \quad (1)$$

Because all two-qubit interactions are mediated by real or virtual transitions amongst the bus eigenstates, suppressing these transitions robustly switches off all interactions mediated by the coupler. As discussed below, if the bus mode is constrained to its ground state, only the virtual transitions of the form $0 \rightarrow n$ need to be suppressed for all n . This mechanism is reminiscent of the strategy used to protect cat qubits from spurious bit flips [23,24,33,34].

An effective Hamiltonian realizing this decoupling mechanism can be put in the form

$$\hat{H} = \sum_{j=1}^2 \hat{H}_j + \hat{H}_b + \hat{H}_r + \sum_{j=1}^2 \hat{H}_{jb} + \hat{H}_{br} + \hat{H}_{br-nl}, \quad (2)$$

where

$$\hat{H}_j/\hbar = \omega_j \hat{q}_j^\dagger \hat{q}_j + \frac{K_j}{2} \hat{q}_j^{\dagger 2} \hat{q}_j^2, \quad (3)$$

$$\hat{H}_b/\hbar = \omega_b \hat{b}^\dagger \hat{b} + \frac{K_b}{2} \hat{b}^{\dagger 2} \hat{b}^2 \quad (4)$$

are the qubits ($j = 1, 2$) and bus Hamiltonians modeled as Kerr-nonlinear oscillators, and

$$\hat{H}_r/\hbar = \omega_r \hat{r}^\dagger \hat{r} - \varepsilon(t) e^{-i\omega_d t} \hat{r}^\dagger - \varepsilon^*(t) e^{i\omega_d t} \hat{r} \quad (5)$$

is the quadratic part of the driven nonlinear resonator Hamiltonian subject to a drive of amplitude $\varepsilon(t)$ and frequency ω_d . In these expressions, $\hat{q}_1, \hat{q}_2, \hat{b}, \hat{r}$ are the annihilation operators of Q_1, Q_2, B , and R with mode frequencies $\omega_1, \omega_2, \omega_b, \omega_r$, and anharmonicities K_1, K_2, K_b and K_r ,

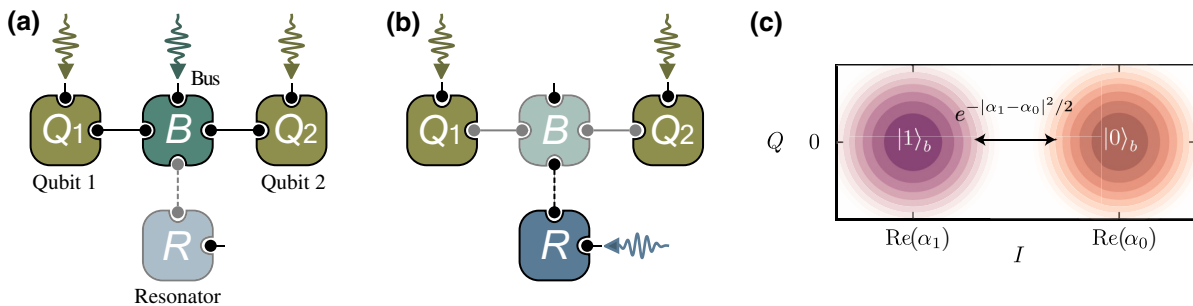


FIG. 2. Illustration of the proposed superconducting coupler. (a) In the *on* state of the coupler the driven nonlinear resonator (R) does not participate in the two-qubit interactions mediated by the bus mode. Local drives on the qubits or bus activate two-qubit gates. (b) In the *off* state, R is subject to a microwave drive that strongly suppresses two-qubit interactions that are mediated by the bus. (c) Metapotential of R for the bus states $|0\rangle_b$ (orange) and $|1\rangle_b$ (purple). Here $\delta/2\pi = -5.0$ MHz, $\chi/2\pi = -20.0$ MHz, and $K_r = 0$. To help visualization, the metapotential $\mathcal{E}(I, Q)$ is renormalized as $\mathcal{E}[(\delta + n\chi)|\alpha_0/4|^2]^{-1}$ for the n th bus state and white corresponds to unity. The global minima of the metapotentials for $n \geq 2$ are close to the global minimum of the $n = 1$ metapotential, but are not shown for simplicity.

respectively. Although our Hamiltonian model is formulated for the case of transmon qubits [35], which can be described as Kerr nonlinear oscillators, our coupling scheme is in principle applicable to other qubit modalities. The qubits interact with the bus mode through a Jaynes-Cummings-type Hamiltonian of the form

$$\hat{H}_{jb}/\hbar = g_j(\hat{q}_j^\dagger \hat{b} + \hat{b}^\dagger \hat{q}_j), \quad (6)$$

where g_j is the coupling strength, while the bus mode interacts with the resonator via the cross-Kerr coupling Hamiltonian

$$\hat{H}_{br}/\hbar = \chi \hat{b}^\dagger \hat{b} \hat{r}^\dagger \hat{r}, \quad (7)$$

which makes the resonator frequency conditional on the bus state via the dispersive shift χ . As will be made clear below, unlike in common circuit QED setups, a large cross-Kerr interaction $|\chi/g_j|$ will be necessary for our protocol. For the last term of Eq. (2), we assume the form

$$\hat{H}_{br-nl}/\hbar = \sum_n \frac{K_r}{2} |n\rangle\langle n|_b \otimes \hat{r}_n^{\dagger 2}(t) \hat{r}_n^2(t), \quad (8)$$

where n runs over all bus states, and $\hat{r}_n(t) = \hat{r} - \alpha_n(t)e^{-i\omega_d t}$. This interaction corresponds to a displaced self-Kerr nonlinearity of the resonator and will be shown to constrain the system dynamics to a low-energy manifold. This synthetic six-wave mixing can be experimentally challenging, but we present a circuit implementation in Sec. V that approximates such a term. Moreover, we show in Sec. IV how to trade this nonlinear interaction for two additional drives on the resonator.

Momentarily ignoring the effect of K_r , the drive on the resonator grows a coherent state of amplitude α_n satisfying

$$i\dot{\alpha}_n(t) = (\delta + n\chi - i\kappa/2)\alpha_n(t) - \varepsilon(t), \quad (9)$$

which, because of the interaction \hat{H}_{br} , is conditional on the bus state $|n\rangle$. Here, $\delta = \omega_r - \omega_d$ is the frequency detuning between the resonator and the drive, and κ is the single-photon loss rate of the resonator. Omitting the qubits, the Hamiltonian of Eq. (2) together with single-photon loss stabilizes joint bus-resonator states of the form $|\psi_{n,k}(t)\rangle = |n\rangle_b |\alpha_n(t)e^{-i\omega_d t}; k\rangle_r$, where $|\alpha; k\rangle_r = e^{\alpha\hat{r}^\dagger - \alpha^*\hat{r}}|k\rangle_r$ is the k th Fock state displaced by an amplitude α . This can be more clearly seen by plotting the metapotential associated with the Hamiltonian \hat{H} with the qubit modes traced out and for $K_r = 0$, obtained by replacing the operator \hat{r} (\hat{r}^\dagger) with the complex variable $I + iQ$ ($I - iQ$). As illustrated in Fig. 2(c), this metapotential has a single well corresponding to a stable point of the system and whose position in the I - Q plane is distinct for each bus state $|n\rangle_b$. Moreover, because the latter states are associated with coherent

states $|\alpha_n\rangle_r$ that are disjoint in phase space, bus transitions are effectively suppressed. If the system is energetically constrained to the first state $|\psi_{n,0}(t)\rangle$ of the metapotential wells, we recover Eq. (1) where the matrix elements of the bus mode are exponentially suppressed with respect to the drive amplitude. The nonlinear interaction \hat{H}_{nlbr} of amplitude K_r plays the role of a self-Kerr nonlinearity within each well of the resonator metapotential. As a result, similarly as in the Kerr-cat qubit [23], this Kerr nonlinearity helps constrain the system's dynamics to the low-energy states of each of the metapotential wells.

Rapid switching between the *on* and *off* states of the coupler is realized by taking advantage of the transitionless-quantum-driving (TQD) method to rapidly displace the coherent state in the resonator starting from vacuum [36]. In the numerical simulations that are discussed below, we use the pulse shape

$$\varepsilon(t) = \left(\varepsilon_0(t) - \frac{i\dot{\varepsilon}_0(t)}{\delta - i\kappa/2} \right) \Theta(\tau - t) + \varepsilon_0(\tau) \Theta(t - \tau), \quad (10)$$

where $\varepsilon_0(t)$ is a smooth drive amplitude, $\varepsilon_0(0) = 0$, and $\Theta(x)$ is the Heaviside step function. With this choice of drive envelope, the steady state reached at time τ takes the form

$$\bar{\alpha}_n \simeq \frac{\varepsilon_0(\tau)}{\delta + n\chi - i\kappa/2} \quad (11)$$

for each bus state $|n\rangle_b$.

To avoid overlapping metapotential wells and strongly suppress the bus transitions $0 \leftrightarrow n$, the system parameters are chosen such that $\bar{\alpha}_0$ is large with respect to any other $\bar{\alpha}_n$. This last requirement ensures that the bus ground state is well separated in energy from the resonator excitations, maximizing the exponential suppression of the two-qubit interaction. More precisely, this is achieved for $|\delta/\chi| \ll 1$ and $|\kappa/\chi| \ll 1$. We note that choosing the drive such as to make $\bar{\alpha}_{n \neq 0}$ large is also a valid strategy. However, we numerically find that increasing $\bar{\alpha}_0$ performs better for small to moderate values of K_r . Importantly, the TQD protocol is reversible and can be used to bring the coupler back to the *on* state by emptying the resonator in a time much faster than $1/\kappa$. The details of this analysis are provided in Appendix A.

III. NUMERICAL EXPERIMENTS

A. Suppression of bus transitions

We now turn to numerical simulations of the concepts presented in the previous section. To illustrate the working principle—the suppression of bus-state transitions in the presence of a drive on the resonator—we first simplify the setup by omitting the qubits. In lieu of the qubits, we add

a drive term of the form

$$\hat{H}_{\text{Rabi}}/\hbar = \Omega(e^{-i\tilde{\omega}_b t}\hat{b}^\dagger + e^{i\tilde{\omega}_b t}\hat{b}), \quad (12)$$

where Ω is the drive amplitude and the drive frequency $\tilde{\omega}_b$ is set to the ac-Stark-shifted 0-1 transition frequency of the bus

$$\tilde{\omega}_b = \omega_b + \frac{\delta(\delta + \chi) - (\kappa/2)^2}{\chi} |\bar{\alpha}|^2 \quad (13)$$

with

$$\bar{\alpha} = \bar{\alpha}_1 - \bar{\alpha}_0 = -\frac{\chi}{\delta + \chi - i\kappa/2} \bar{\alpha}_0 \quad (14)$$

being the distance between the metapotential wells associated with the ground and first excited states of the bus. In the *on* state of the coupler, the resonant drive on the bus will result in Rabi oscillations between $|0\rangle_b$ and $|1\rangle_b$. In the *off* state, bus transitions, and therefore Rabi oscillations, are exponentially suppressed with the coherent state amplitude $\bar{\alpha}_0$.

Indeed, according to Eq. (1), we expect the Rabi frequency in the presence of a drive on the resonator to take the form

$$\tilde{\Omega} \approx \Omega \exp(-|\bar{\alpha}|^2/2). \quad (15)$$

Following Eq. (14), $|\bar{\alpha}|$ is bounded by $|\bar{\alpha}_0|$. Indeed, $0 \leq |\bar{\alpha}| < |\bar{\alpha}_0|$ where the lower bound corresponds to $\chi = 0$ or $\bar{\alpha}_0 = 0$, and the upper bound is reached for $|\chi| \rightarrow \infty$. As a result, increasing $|\chi|$ results in a stronger suppression of $\tilde{\Omega}$.

Figure 3(a) shows the Rabi frequency $\tilde{\Omega}$ obtained from numerical integration of the coupler master equation based on Eq. (2). The result includes damping in the resonator but excludes decoherence in the bus, and it is computed for different equilibrium values of $|\bar{\alpha}_0|^2$ and cross-Kerr interactions χ . The data points are extracted from fits to the bus population $\langle \hat{b}^\dagger \hat{b} \rangle(t)$ with the bus and resonator initialized to the vacuum state; see panel (c). The numerical result (symbols) is in excellent agreement with Eq. (15) (dashed lines) and displays the expected exponential suppression of the bus Rabi oscillations. This suppression becomes more significant for increasing cross-Kerr coupling $|\chi|/2\pi$ that is shown here ranging from 5 to 20 MHz. We note that these results are obtained for $K_r = 0$. In the absence of the qubits ($g_j = 0$), choosing small $|\Omega/\delta|$ guarantees that the dynamics is mainly generated by states $|\psi_{n,0}\rangle$ for which the exponential suppression of the Rabi frequency is maximized. Indeed, the states $|\psi_{0,k}\rangle$ are separated in energy by δ and, thus, to prevent transitions to $k \neq 0$ states during a $1 \rightarrow 0$ bus transition, we ideally require the matrix elements of Rabi drive Hamiltonian in the state basis $|\psi_{n,k}\rangle$ to be small relative to δ , i.e., $|\Omega \langle \psi_{0,k} | \hat{b} | \psi_{1,0} \rangle / k\delta| = |\tilde{\Omega} \bar{\alpha}^k / k\delta\sqrt{k!}| \ll 1$ for $k \neq 0$.

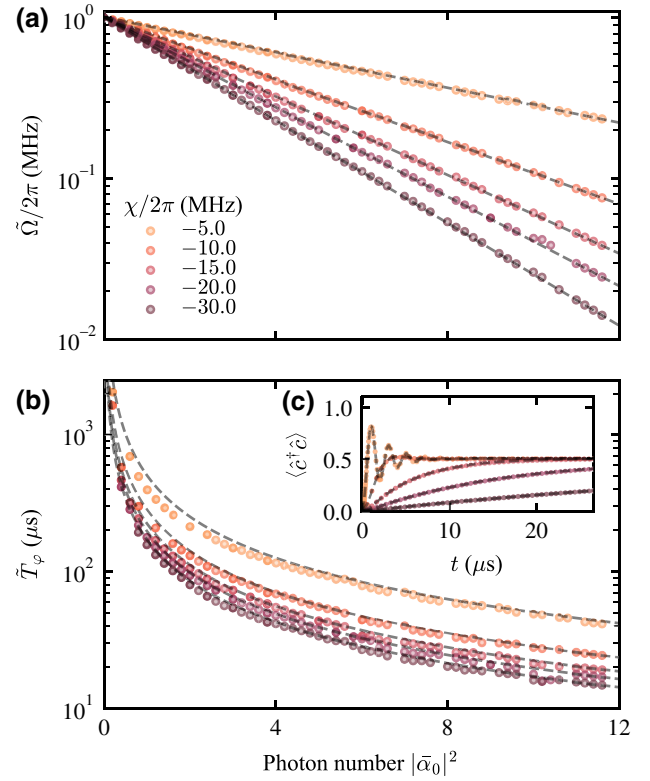


FIG. 3. Renormalized bus (a) Rabi frequency $\tilde{\Omega}/2\pi$ and (b) dephasing time \tilde{T}_φ under a resonant $\Omega/2\pi = 1$ MHz microwave bus drive as a function of the photon number in the resonator, $|\bar{\alpha}_0|^2$. The results are obtained using a 5-ns-long TQD scheme with $\kappa/2\pi = 100$ KHz, $\delta/2\pi = -5$ MHz, $K_b/2\pi = -300$ MHz. The cross-Kerr $\chi/2\pi$ is varied in the range -5.0 to -30.0 MHz. Fits are done by comparing the time evolution to that of an effective two-level system, including both T_1 and T_2 . Dashed lines correspond to Eqs. (15) and (16). (c) Example of the time-evolution traces that are fitted for $|\bar{\alpha}_0|^2 = 11$.

In the presence of single-photon loss in the resonator, the distinct coherent states associated with the different bus states lead to bus dephasing. This originates from the “which-bus-state” information that is carried by the lost photons, something that is akin to measurement-induced dephasing in the dispersive readout of circuit QED [37]. With T_φ denoting the bare bus dephasing time, the coherence time in the presence of the resonator drive takes the form

$$\tilde{T}_\varphi \approx \left(\frac{1}{T_\varphi} + \frac{\kappa}{2} |\bar{\alpha}|^2 \right)^{-1}. \quad (16)$$

Figure 3(b) shows this dephasing time extracted from the numerical simulations including $\kappa \neq 0$ [symbols]. Similarly to the previous case, we find excellent agreement with the analytical expression (dashed lines). To isolate the effects of resonator dissipation on the system, we have omitted intrinsic relaxation and dephasing of the bus mode.

A key observation is that, while transitions between the bus states are suppressed exponentially with $\bar{\alpha}$, dephasing only increases polynomially with this quantity. Moreover, we demonstrate below that the dephasing induced on the bus mode does not percolate to the qubits.

B. Suppression of two-qubit interactions

Having numerically confirmed that suppressing the bus transitions by driving the resonator is possible, we now reintroduce the qubits to the model and explore the two-qubit decoupling. In particular, we characterize the hybridization between the qubit and bus modes as a function of the resonator drive parameters and demonstrate how spurious two-qubit couplings, such as the ZZ interaction, are exponentially suppressed.

We now take $K_r \neq 0$ in Eq. (2). In the presence of this term, Eqs. (5), (7), and (8) still stabilize displaced Fock states in the resonator, with displacement $\alpha_n(t)e^{-i\omega_d t}$. The driven states in the nonlinear resonator are therefore unchanged under the action of Eq. (8). As is discussed below, the role of the nonlinearity K_r is instead to constrain the resonator to low-energy states.

1. Polaron transformation

Analyzing the underlying physics of the model Hamiltonian is made easier after a rotating-frame transformation and a polaronlike transformation that displaces the resonator mode conditionally on the state of the bus. Acting with Eq. (A1) on Eq. (2), the transformed Hamiltonian takes the form (see Appendix A)

$$\hat{H}^P = \sum_{j=1}^2 \hat{H}_j^P + \hat{H}_{br}^P + \hat{H}_\kappa^P + \hat{H}_g^P \quad (17)$$

with

$$\hat{H}_j^P/\hbar = \tilde{\Delta}_j \hat{q}_j^\dagger \hat{q}_j + \frac{K_j}{2} \hat{q}_j^{\dagger 2} \hat{q}_j^2, \quad (18)$$

$$\hat{H}_{br}^P/\hbar = (\delta + \chi \hat{b}^\dagger \hat{b}) \hat{r}^\dagger \hat{r} + \frac{\tilde{K}_b}{2} \hat{b}^{\dagger 2} \hat{b}^2 + \frac{K_r}{2} \hat{r}^{\dagger 2} \hat{r}^2, \quad (19)$$

$$\hat{H}_\kappa^P/\hbar = \frac{i\kappa}{2} \sum_n (\alpha_n \hat{r}^\dagger - \alpha_n^* \hat{r}) |n\rangle \langle n|_b, \quad (20)$$

$$\hat{H}_g^P/\hbar = \sum_{j,n} g_j \hat{q}_j^\dagger e^{i\phi_n} \hat{D}_{n,r} \sqrt{n+1} |n\rangle \langle n+1|_b + \text{H.c.}, \quad (21)$$

where the resonator decay rate κ appears in the displacement transformation according to Eq. (9). In \hat{H}_g^P we have

defined the bus-state-dependent phases

$$\phi_n = \frac{\alpha_{n+1}^* \alpha_n - \alpha_n^* \alpha_{n+1}}{2i}, \quad (22)$$

the resonator displacement operators

$$\hat{D}_{n,r} = e^{(\alpha_{n+1} - \alpha_n) \hat{r}^\dagger - (\alpha_{n+1}^* - \alpha_n^*) \hat{r}}, \quad (23)$$

and the ac-Stark-shifted qubit-bus detunings and bus anharmonicity

$$\begin{aligned} \tilde{\Delta}_j &= \omega_j - \omega_b - \delta |\alpha_0|^2 + (\delta + \chi) |\alpha_1|^2, \\ \tilde{K}_b &= K_b - \delta |\alpha_0|^2 + 2(\delta + \chi) |\alpha_1|^2 - (\delta + 2\chi) |\alpha_2|^2, \end{aligned} \quad (24)$$

respectively. In what follows, we neglect the transients to focus on times where the polaronic states are fully grown with $\alpha_n = \bar{\alpha}_n$ as defined in Eq. (11).

In the polaron frame Hamiltonian \hat{H}^P , all modes are described by a Kerr nonlinear oscillator Hamiltonian. Moreover, the interaction between the qubits and the bus, \hat{H}_g^P , reflects the fact that transitions in the bus are accompanied by displacements of the resonator field. Damping is described by the usual Lindblad master equation, now expressed in the polaron frame as discussed in Appendix 2. In particular, the resonator photon-loss Lindblad operator $\hat{L}_r = \sqrt{\kappa} \hat{r}$ in the laboratory frame transforms to $\hat{L}_r^P = \sqrt{\kappa} (\hat{r} + \sum_n \bar{\alpha}_n |n\rangle \langle n|_b)$ in the polaron frame. The action of both \hat{H}_κ^P and \hat{L}_r^P ensures the stabilization of the vacuum state in the resonator for all $|n\rangle_b$. Under the rotating-wave approximation, the Lindblad dynamics of the system can be further reduced to the effective Hamiltonian $\hat{H}^P - \hat{H}_\kappa^P$ together with the two Lindblad operators $\sqrt{\kappa} \hat{r}$ and $\sqrt{\kappa} \sum_n \bar{\alpha}_n |n\rangle \langle n|_b$. By assuming the dynamics to be restrained to the ground and first excited states of the bus, the latter operator takes the simpler form (cf. Appendix A)

$$\hat{L}_b^P = \sqrt{\frac{\kappa |\bar{\alpha}|^2}{4}} (|1\rangle \langle 1|_b - |0\rangle \langle 0|_b). \quad (26)$$

This result is in agreement with the expression for the bus dephasing time of Eq. (16).

2. Inverse participation ratio

A useful quantity to further characterize the exponential suppression of the two-qubit interactions is the mode hybridization between the qubits and the bus in the *off* state. To quantify this effect, we make use of the inverse participation ratio (IPR) [38,39], which here takes the form

$$\eta_\mu := \frac{\sum_\nu |\langle \psi_{h,\mu} | \psi_{b,\nu} \rangle|^4}{|\langle \psi_{h,\mu} | \psi_{h,\mu} \rangle|^2}, \quad (27)$$

where $|\psi_{b,\nu}\rangle$ and $|\psi_{h,\nu}\rangle$ are the bare ($g_j = 0$) and hybridized ($g_j \neq 0$) eigenstates of the full system. The IPR

is a measure of how localized the wavefunctions of the circuit modes are with respect to the bare modes, and it ranges from $1/4$ (maximally delocalized states) to 1 (maximally localized states) for our system with four modes.

In the dispersive regime where the qubits are largely detuned from the bus mode, analytical expressions for η_μ can be obtained by eliminating \hat{H}_g^P in \hat{H}^P using a Schrieffer-Wolff transformation. For the bare states $|\psi_{b,v}\rangle$ with $v \in \{1000, 0100, 1100\}$ and where the state indexing corresponds to (Q_1, Q_2, B, R) , we obtain in Appendix 2

$$\eta_{1000} \approx 1 - 2e^{-|\bar{\alpha}|^2} \left(\frac{g_1}{\tilde{\Delta}_1} \right)^2 {}_4F_4(\mathbf{p}_1; 1 + \mathbf{p}_1; |\bar{\alpha}|^2), \quad (28)$$

$$\eta_{0100} \approx 1 - 2e^{-|\bar{\alpha}|^2} \left(\frac{g_2}{\tilde{\Delta}_2} \right)^2 {}_4F_4(\mathbf{p}_2; 1 + \mathbf{p}_2; |\bar{\alpha}|^2), \quad (29)$$

and $\eta_{1100} \approx \eta_{1000} + \eta_{0100} - 1$, where $\bar{\alpha} = \bar{\alpha}_1 - \bar{\alpha}_0$, ${}_pF_q$ is the generalized hypergeometric function, $\mathbf{p}_j = (p_{j-}, p_{j-}, p_{j+}, p_{j+})$ with $p_{j\pm} = \beta[1 \pm \sqrt{1 + 2\tilde{\Delta}_j\beta^{-2}/K_r}]$, and $\beta = (\delta + \chi)/K_r - 1/2$. The expressions for η_μ show that the degree of mode hybridization decreases with increasing detuning. More importantly, we also see that hybridization is exponentially suppressed with increasing photon population of the resonator mode. At large photon number, virtual transitions to higher-energy states within the resonator's metapotential wells can impact the level of exponential suppression, something that is represented by the contribution from the hypergeometric function. These higher-energy transitions can, however, be prevented by increasing $|\delta + \chi|$ and $|K_r|$.

To verify these observations, we investigate the quantity $1 - \eta_{1000}$ as a function of the photon number $|\bar{\alpha}_0|^2$ in the resonator by exact diagonalization of the Hamiltonian of Eq. (17) for $\kappa = 0$ (see Fig. 4). Different colors correspond to different values of the nonlinearity K_r . Focusing first on panel (a), obtained for $\delta/2\pi = -1.5$ MHz, the anticipated suppression of the hybridization with increasing $|\bar{\alpha}_0|^2$ is clearly observed, together with the slowdown of that trend for larger $|\bar{\alpha}_0| \propto |\bar{\alpha}|$.

The shaded region is plotted using the analytical expression in Eq. (28) for K_r in the range $|K_r| \rightarrow \infty$ to $K_r = 0$. In the former limit, the dynamics is constrained to the low-lying polaronic states, i.e., the resonator is constrained to the displaced Fock states $|0\rangle$ and $|1\rangle$ in the laboratory frame, and the exponential suppression persists for large $|\bar{\alpha}_0|$. As a comparison, the dashed line is obtained from the usual dispersive factor $(g_i/\tilde{\Delta}_i)^2$, taking into account the change in qubits-bus detuning due to the ac-Stark shift and that corresponds to usual qubit-bus-qubit couplers without the driven resonator. The very strong suppression of $1 - \eta_{1000}$ observed in Fig. 4(a) for our coupler design has an important consequence: because of the very small

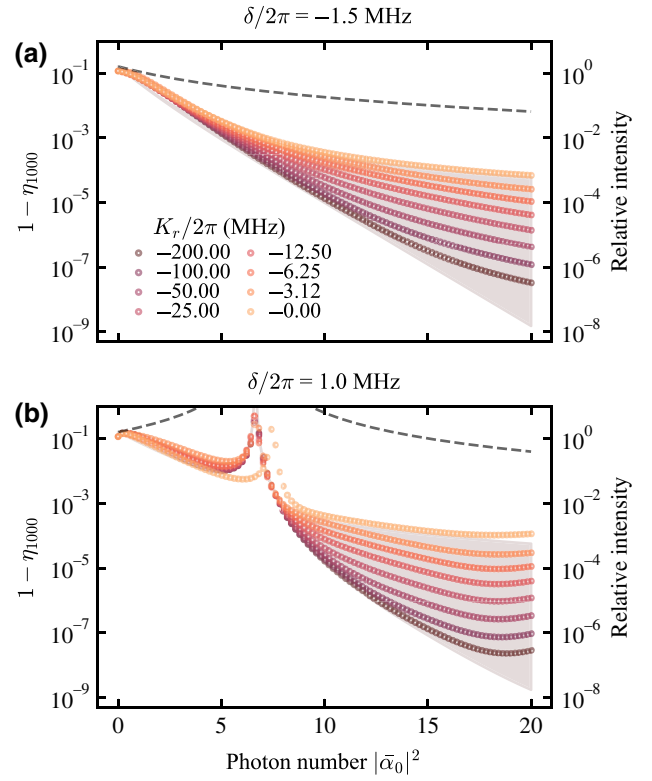


FIG. 4. Suppression of $1 - \eta_{1000}$ with respect to the resonator photon number $|\bar{\alpha}_0|^2$ for (a) $\delta/2\pi = -1.5$ MHz and (b) $\delta/2\pi = 1.0$ MHz. The data points are obtained from numerical diagonalization with a fixed drive amplitude in the resonator. Analogous plots for $1 - \eta_{0100}$ can be found in Appendix 2. Dashed lines correspond to the same system but with the resonator undriven and the bus frequency tuned to the ac-Stark-shifted frequency found in the driven system. The gray regions are bounded by the analytical estimates in Eq. (28) for $K_r \rightarrow \infty$ and $K_r = 0$. Here $(\omega_1 - \omega_b)/2\pi = 7.0$ MHz, $(\omega_2 - \omega_b)/2\pi = 14.0$ MHz, $K_1/2\pi = K_2/2\pi = -300.0$ MHz, $\chi/2\pi = -20.0$ MHz, and $g/2\pi = 2.0$ MHz.

hybridization of the qubit eigenstates, all real and virtual qubit-qubit interactions mediated by the coupler are exponentially suppressed in amplitude; see Appendix 4 for details. Analogous plots for $1 - \eta_{0100}$ can be found in Appendix 2.

Figure 4(b) also shows $1 - \eta_{1000}$ as a function of the number of photons $|\bar{\alpha}_0|^2$ in the resonator but now for a positive detuning of $\delta/2\pi = 1$ MHz. In this situation, we observe a divergence in $1 - \eta_{1000}$ associated with a resonance in the ac-Stark-shifted detunings $\tilde{\Delta}_1$. As discussed in Appendix 6, this resonance can be understood from the poles of the generalized hypergeometric function appearing in Eqs. (28) and (29), which correspond to frequency collisions with higher-energy levels of the resonator. For negative detunings δ , these collisions are avoided and the suppression is monotonic with photon number. On the other hand, choosing $\delta > 0$ results in a nonmonotonic $1 -$

η_{1000} , something that can lead to a stronger suppression of unwanted interactions. See Appendix 6 for a detailed discussion of these frequency collisions and how to take advantage of them.

As previously alluded to, the exponential suppression of qubit-qubit interactions is greatly enhanced at large photon numbers in the resonator if the $|\tilde{\Delta}_j/\chi|$ or $|\tilde{\Delta}_j/K_r|$ are small. These ratios determine the probability of a resonance with higher-energy levels of the resonator. Because the latter tend to cover a larger area in the phase space of the resonator than the low-energy states, their occupation would attenuate the exponential suppression of qubit-qubit interactions. We highlight that taking $|\tilde{\Delta}_j/\chi|$ or $|\tilde{\Delta}_j/K_r|$ small is a natural parameter regime with protected qubits, which often have small frequencies by design [23,26]. This feature underlines the compatibility of our coupler with protected qubits.

We conclude this section with a remark regarding the optimal ramping rate ν of the photon number, i.e., $|\bar{\alpha}_0(t)|^2 = \nu t$, to minimize the impact of accidental resonances. Frequency collisions in Figs. 4 and 9 correspond to pairs of qubit-coupler states that are brought into resonance as the coherent state amplitude goes from 0 to $\bar{\alpha}_0$. As detailed in Appendix 3, as the levels go through the crossing, the state of the qubit leaks to the coupler following the Landau-Zener formula [40] and, as a result, the probability of leakage is exponentially reduced in $|\nu/g'_j|$, where g'_j is the effective coupling strength between Q_j and B that is exponentially suppressed in $|\bar{\alpha}_0|$. However, nonadiabatic errors in the TQD protocol, determined by ratios of the pulse's time derivatives to the cross-Kerr interaction strength χ (cf. Appendix A), impose an upper bound on ν . Near that upper bound, the leakage probability is nonetheless exponentially suppressed in both $|\bar{\alpha}_0|^2$ and $|\chi/g'_j|$, as inferred in Appendix 3. We highlight that $|g'_j/\chi| \ll 1$ was already a key requirement for the proposed device.

3. Suppression of spurious interactions

We now analyze how the proposed coupler helps to suppress the spurious cross-Kerr coupling between the qubits, which is given by

$$\chi_{12} = \omega_{1100} - \omega_{1000} - \omega_{0100} + \omega_{0000}, \quad (30)$$

where $\omega_\mu = \langle \psi_{h,\mu_\star} | \hat{H}^P - \hat{H}_\kappa^P | \psi_{h,\mu_\star} \rangle$ is the energy associated with the two-qubit eigenstate $|\psi_{h,\mu_\star}\rangle$ with maximal overlap with the bare state $|\psi_{b,\mu}\rangle$, i.e., $\mu_\star = \text{argmax}_\nu |\langle \psi_{h,\nu} | \psi_{b,\mu} \rangle|^2$.

Figure 5 shows $|\chi_{12}|$ obtained from numerical diagonalization of $\hat{H}^P - \hat{H}_\kappa^P$ as a function of $|\bar{\alpha}_0|^2$ for different values of K_r (symbols). As a comparison, the dashed line shows $|\chi_{12}|$ resulting only from the change in detuning between the qubits and the bus due to the ac-Stark shift,

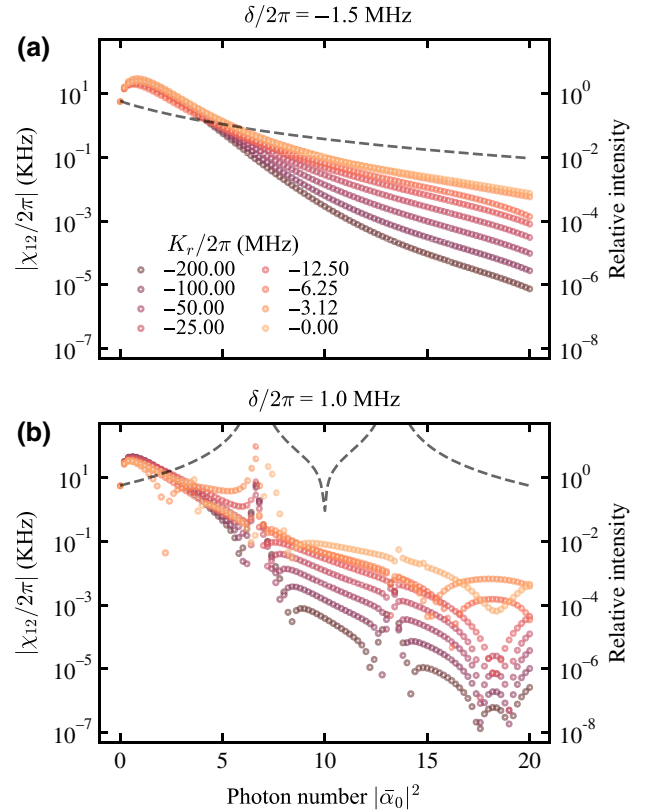


FIG. 5. Suppression of the ZZ interaction χ_{12} between the qubits as a function of the resonator photon number $|\bar{\alpha}_0|^2$ for (a) $\delta/2\pi = -1.5$ MHz and (b) $\delta/2\pi = 1.0$ MHz. Data points correspond to numerical diagonalization of the system Hamiltonian with a fixed drive amplitude in the resonator. Dashed lines correspond to Eq. (31), i.e., the same system but with the resonator undriven and the bus frequency tuned to the ac-Stark-shifted frequency found in the driven system. Here $(\omega_1 - \omega_b)/2\pi = 7.0$ MHz, $(\omega_2 - \omega_b)/2\pi = 14.0$ MHz, $K_1/2\pi = K_2/2\pi = -300.0$ MHz, $\chi/2\pi = -20.0$ MHz, and $g/2\pi = 2.0$ MHz.

and computed using the perturbative expression

$$\chi_{12}^{\text{ac}} = \frac{1}{6} \frac{g_1^2}{\tilde{\Delta}_1} \frac{g_2^2}{\tilde{\Delta}_2} \left(\frac{1}{\tilde{\Delta}_1} + \frac{1}{\tilde{\Delta}_2} \right), \quad (31)$$

valid for $|\tilde{\Delta}_j/K_j| \ll 1$ and $|\tilde{\Delta}_j/\tilde{K}_b| \ll 1$. The latter is obtained from a Magnus expansion to fourth order in the coupling strengths (cf. Appendix 4). The two resonances observed in the dashed line and the numerical data in panel (b) correspond to $\tilde{\Delta}_j = 0$.

As first noted for $1 - \eta_{1000}$ in Fig. 4, the suppression of χ_{12} is monotonic with photon number for negative detunings δ [panel (a)], while some nonmonotonic features appear at positive detuning where the suppression is also stronger [panel (b)]. See Appendix 6 for a discussion of the origin of these features.

We also note the presence of more features in Fig. 5(b) for χ_{12} than in Fig. 4(b) for $1 - \eta_{1000}$. The first two dominant peaks in Fig. 5(b) result from accidental resonances between each qubit and the bus, i.e., $\tilde{\Delta}_j = 0$, in agreement with the peaks observed for $1 - \eta_{1000}$ in Fig. 4 and $1 - \eta_{0100}$ in Fig. 9. Additional features in Fig. 5 not present in Figs. 4 and 9 result from frequency collisions with higher-energy levels in the system, activated by the ac-Stark shifts in the bus.

Importantly, the suppression of $1 - \eta_\mu$ and the resulting reduction of the spurious cross-Kerr coupling does not require fine tuning of the circuit or drive parameters. Indeed, as illustrated in Figs. 4 and 5, strong suppression is observed for different choices of circuit parameters, including δ and K_r . It is also worth emphasizing that all real and virtual interactions are suppressed by this scheme. This fact is in stark contrast to other approaches where cancellation of two-qubit interactions is realized only for a precise value of a control parameter and where residual virtual interactions such as χ_{12} remain present [5,21,22].

Finally, we note that it is possible to combine our coupler with other approaches for suppressing spurious interactions, for instance by using qubits with opposite sign anharmonicities [21,22].

C. Bus-induced qubit dephasing

At the origin of the suppression of unwanted interaction are the disjoint bus-state-dependent coherent states of the driven resonator. A photon lost from the resonator carries the “which-bus-state” information and leads to dephasing of the bus state. Because there exists hybridization between the bus and qubit modes, this mechanism can introduce additional qubit dephasing. However, as shown in more detail in Appendix A, we find that this is not an important contribution to qubit dephasing. Indeed, by expressing Eq. (26) in the hybridized eigenbasis, the dephasing rate of the first qubit is given by

$$\begin{aligned} \gamma_{\phi,1} &= \frac{\kappa |\bar{\alpha}|^2}{2} \left(\sum_{k=0}^{\infty} |\langle \psi_{h,1000} | \psi_{b,001k} \rangle|^2 \right)^2 \\ &\approx \frac{\kappa |\bar{\alpha}|^2}{2} \frac{1 - \eta_{1000}}{2}, \end{aligned} \quad (32)$$

where the second line follows from a Schrieffer-Wolff transformation (cf. Appendix 5). The expression above is obtained with a rotating-wave approximation, which is valid for $|\gamma_{\phi,1}/\tilde{\Delta}_1| \ll 1$. An expression for the second qubit is obtained by simply replacing the subscript 1000 by 0100.

Similarly to measurement-induced dephasing [37], the prefactor of Eq. (32) scales with the photon number $|\bar{\alpha}|^2$ in the resonator. However, because $1 - \eta_\mu$ is exponentially suppressed with increasing $|\bar{\alpha}|^2$, the qubit dephasing rate can be made negligible in the *off* state of the coupler.

Appendix 5 also compares Eq. (32) versus photon number against the result obtained from numerical diagonalization of $\hat{H}^P - \hat{H}_\kappa^P$. As with the suppression of unwanted ZZ interactions, the reason for this negligibly small dephasing rate is the very low hybridization of the qubits’ eigenstates with the bus and resonator modes.

IV. EFFECTIVE PARAMETRIC MODULATION

In the previous sections, we have seen that large nonlinear interaction amplitudes K_r help in the suppression of the unwanted interactions in the *off* state of the coupler. Here, we explore an alternative strategy that relies on a two-tone drive on the resonator. Moreover, because the nonlinearity is not needed in this case, the resonator can be taken to be a linear resonator (LR). This might also simplify the experimental realization of these ideas.

Our starting point is again the Hamiltonian of Eq. (2) where we now take $K_r = 0$ and introduce the following additional drive on the LR:

$$\hat{H}_{\text{DD}} = -\frac{i\lambda\omega_m}{2\bar{\alpha}^*} [e^{-i(\omega_r - \omega_m)t} - e^{-i(\omega_r + \omega_m)t}] \hat{r}^\dagger + \text{H.c.}, \quad (33)$$

where DD stands for dynamical decoupling.

Here λ is a real-valued amplitude and the frequency ω_m is assumed here to be much larger in magnitude than the cross-Kerr interaction χ . With this additional two-tone drive on the LR, the steady-state bus-dependent coherent state Eq. (11) becomes

$$\bar{\alpha}_n \rightarrow \bar{\alpha}_n - i\lambda \cos(\omega_m t) / \bar{\alpha}^*, \quad (34)$$

where λ plays the role of the amplitude of a modulation around the steady-state value $\bar{\alpha}_n$. Crucially, this modulation changes the phase ϕ_n that specifies the bus-state-dependent displacements Hamiltonian \hat{H}_g^P in Eq. (21), which can now be written as

$$\phi_n(t) = \bar{\phi}_n - \lambda \text{Re} \left[\frac{\bar{\alpha}_{n+1} - \bar{\alpha}_n}{\bar{\alpha}} \right] \cos(\omega_m t), \quad (35)$$

$$\bar{\phi}_n = \frac{\bar{\alpha}_{n+1}^* \bar{\alpha}_n - \bar{\alpha}_n^* \bar{\alpha}_{n+1}}{2i}. \quad (36)$$

Moreover, the qubit-bus detunings transform to $\tilde{\Delta}_j = \tilde{\Delta}_j^0 + \tilde{\Delta}_j^t$, where

$$\tilde{\Delta}_j^0 = \omega_j - \omega_b - \delta |\bar{\alpha}_0|^2 + (\delta + \chi) |\bar{\alpha}_1|^2 + \frac{\chi \lambda^2}{2|\bar{\alpha}|^2}, \quad (37)$$

$$\tilde{\Delta}_j^t = -2\chi \lambda \text{Im} \left[\frac{\bar{\alpha}_1}{\bar{\alpha}} \right] \cos(\omega_m t) + \frac{\chi \lambda^2}{2|\bar{\alpha}|^2} \cos(2\omega_m t). \quad (38)$$

An additional rotating-frame transformation such as to remove the time dependence of the qubit-bus detunings,

leads to the following approximation for \hat{H}_g^P :

$$\hat{H}_g^P = \sum_{j,n} g_j \hat{q}_j^\dagger e^{i\phi_n'(t)} \hat{D}_{n,r} \sqrt{n+1} |n\rangle \langle n+1|_b + \text{H.c.} \quad (39)$$

Here we have introduced $\phi_n'(t) = \phi_n(t) + \int_0^t dt \tilde{\Delta}_j^t$. Except for the now time-dependent phase $\phi_n'(t)$, Eq. (39) has the same form as Eq. (21).

The role of the time-dependent phase $\phi_n'(t)$ can be understood by using the Jacobi-Anger expansion

$$e^{i\phi_n'} = e^{i\tilde{\phi}_n} \sum_{s=-\infty}^{+\infty} (-i)^s J_s \left(\lambda \operatorname{Re} \left[\frac{\tilde{\alpha}_{n+1} - \tilde{\alpha}_n}{\tilde{\alpha}} \right] \right) e^{is\omega_m t}, \quad (40)$$

where $J_s(z)$ is the s th Bessel function of the first kind, and where we considered negligible χ/ω_m for simplicity. Because the bus mode is ideally only virtually excited at all times, our goal is to dominantly suppress the $0 \leftrightarrow 1$ transition in the bus. To achieve this, we adjust the amplitude λ to reach a zero of J_0 in Eq. (40), noting that $\tilde{\alpha} = \tilde{\alpha}_1 - \tilde{\alpha}_0$. Higher harmonics of Eq. (40) oscillate rapidly for $\omega_m \gg |\chi|, |\tilde{\Delta}_j^0|$, and result in a lower bound on the suppression of the two-qubit interactions (cf. Appendix C).

To understand how the two proposed implementation mechanisms compare to each other, we compute in Appendix 2 the quantity $1 - \eta_\mu$ using a time-dependent Schrieffer-Wolff transformation to find that

$$1 - \eta_{1000} \approx 2g_1^2 e^{-|\tilde{\alpha}|^2} \sum_{s_1, s_2 = -\infty}^{+\infty} i^{s_2 - s_1} e^{i(s_2 - s_1)\omega_m t} \times J_{s_1}(\lambda) J_{s_2}(\lambda) \frac{4F_4(\mathbf{p}_{1s_1 s_2}; 1 + \mathbf{p}_{1s_1 s_2}; |\tilde{\alpha}|^2)}{(\tilde{\Delta}_1^0 + s_1 \omega_m)(\tilde{\Delta}_1^0 + s_2 \omega_m)}, \quad (41)$$

where $\mathbf{p}_{j_1 j_2} = (p_{j_1 -}, p_{j_2 -}, p_{j_1 +}, p_{j_2 +})$ with $p_{j_\pm} = \beta[1 \pm \sqrt{1 + 2(\tilde{\Delta}_j^0 + s\omega_m)\beta^{-2}/K_r}]$ and $\beta = (\delta + \chi)/K_r - 1/2$. We observe that Eq. (41) is reminiscent of Eq. (28), and a similar expression for η_{100} can be derived. In the large $\omega_m \gg |\tilde{\Delta}_1^0|$ limit, the dominant contribution to Eq. (41) arises from the term with $s_1 = s_2 = 0$, which is canceled by adjusting λ to reach a zero of J_0 . Importantly, because of the already suppressed interactions, there is no need for a very fine adjustment of λ . The time averaged $1 - \eta_{1000}$ according to Eq. (41) is illustrated in Fig. 6, where we take $\omega_m = \omega_0 |\tilde{\alpha}|$ such that the drive amplitude in Eq. (33) is independent of $|\tilde{\alpha}|$. The dashed line corresponds to the absence of dynamical decoupling. The shaded regions correspond to $\pm 10\%$ error bounds on the drive amplitude. We observe a strong suppression of $1 - \eta_{1000}$ and of the drive amplitude sensitivity. As discussed further in Appendix C, we note that the asymptotic behavior of the suppression is polynomial in $\tilde{\alpha}$. With the very large suppression of

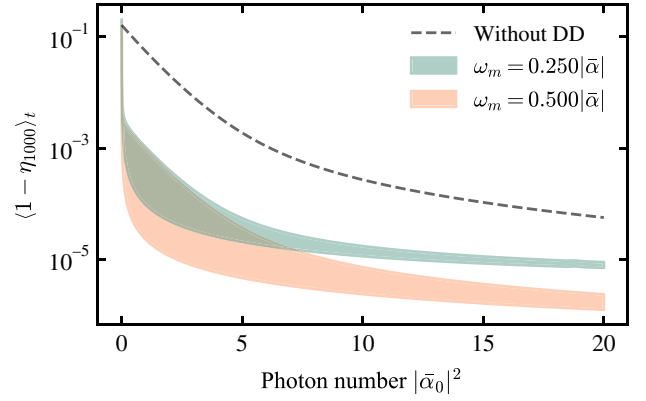


FIG. 6. Time-averaged inverse participation ratio against photon number using a two-tone drive on the LR ($K_r = 0$) with frequencies $\omega_r \pm \omega_m$ and amplitudes $\omega_m \lambda / \tilde{\alpha}^*$. The shaded regions are bounded by $\lambda = \lambda_0$, where $J_0(\lambda_0) = 0$, and a 10% error on λ_0 . The other parameters are $\delta/2\pi = -1.0$ MHz, $\chi/2\pi = -20.0$ MHz, $(\omega_1 - \omega_b)/2\pi = 7.0$ MHz, $(\omega_2 - \omega_b)/2\pi = 14.0$ MHz, $K_1/2\pi = K_2/2\pi = -300.0$ MHz, and $g/2\pi = 2.0$ MHz. See Appendix C for $\langle 1 - \eta_{0100} \rangle_t$.

$1 - \eta_\mu$ that is observed in Fig. 6, this is a small price to pay when trading the nonlinearity K_r for an additional drive. We finally note that the suppression can be further enhanced with the help of a longitudinal drive in the LR (cf. Appendix C).

V. SUPERCONDUCTING CIRCUIT IMPLEMENTATION

In this section, we introduce a superconducting quantum circuit realizing our coupler. To approach the model Hamiltonian of Eq. (2), we draw inspiration from the Kerr-cat qubit that exploits the bifurcation physics of driven Josephson-based devices [23,24]. A simplification, based on the idea of dynamical decoupling in Sec. IV, is also discussed.

A. Kerr-cat-based circuit model

Figure 7(a) shows a possible circuit realization of our coupler with two transmon qubits interacting through a transmonlike device playing the role of bus mode. The latter is connected to a driven nonlinear circuit representing the resonator and consisting here of a loop formed by two symmetrical Josephson junctions and a snail-like element incorporates an array of $N \sim 3$ junctions [3]. As mentioned earlier, although for simplicity we focus here on transmon qubits, this scheme is applicable to other types of superconducting and, in particular, is well adapted to protected qubits.

Omitting the qubits for the moment, the Hamiltonian of the circuit reads

$$\hat{H} = \hat{H}_b + \hat{H}_r + \hat{H}_{br}, \quad (42)$$

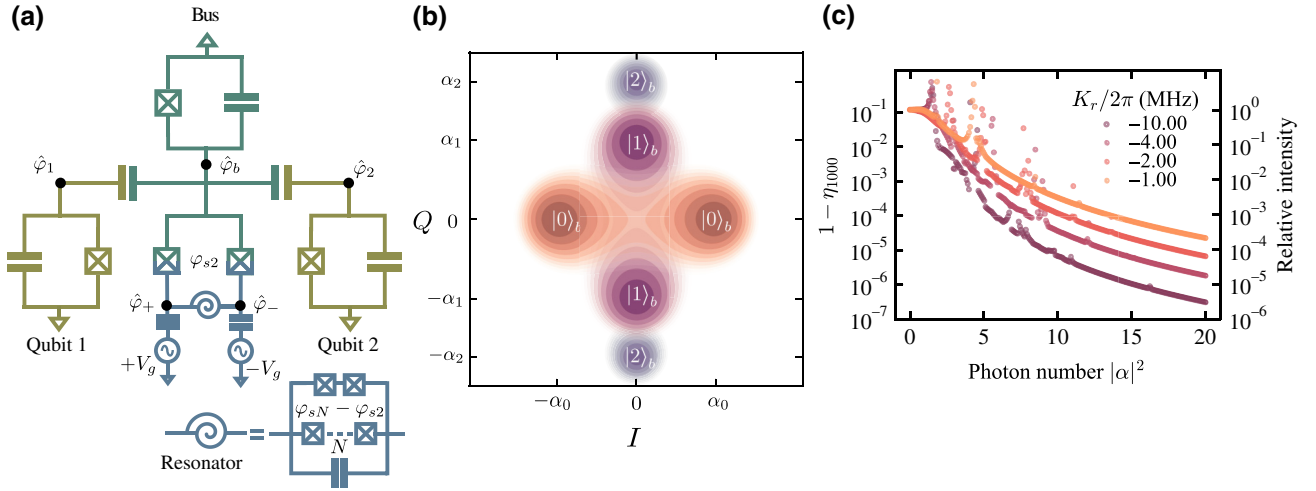


FIG. 7. Superconducting circuit implementation. (a) Circuit design. The qubits and bus modes are implemented using transmon qubits; $\hat{\varphi}_1$, $\hat{\varphi}_2$, and $\hat{\varphi}_b$ are the phase operators of Q_1 , Q_2 , and the bus modes, respectively. Here $2\hat{\varphi}_\pm = -\hat{\varphi}_b \pm (\hat{\varphi}_r - \varphi_\ell)$, where φ_ℓ is a real-valued scalar to be defined. A snail-like element, representing the resonator mode with phase operator $\hat{\varphi}_r$, is linearly driven by a voltage source V_g . The two external fluxes $\Phi_0\varphi_{s2}/2\pi$ and $\Phi_0(\varphi_{sN} - \varphi_{s2})/2\pi$ control the bus-resonator interaction. (b) Metapotential of the resonator for each of the bus states $|0\rangle_b$ (orange), $|1\rangle_b$ (purple), and $|2\rangle_b$ (blue). Here $\delta/2\pi = -5.0$ MHz, $\chi/2\pi = -5.0$ MHz, and $K_r/2\pi = -10.0$ MHz. (c) The quantity $1 - \eta_{1000}$ (and $1 - \eta_{0100}$ can be found in Appendix D) estimated by numerical diagonalization of the full system using the effective Hamiltonian in Eq. (53) with $\delta/2\pi = 1$ KHz, $\chi/2\pi = -5.0$ MHz, $(\omega_1 - \omega_b)/2\pi = 7.0$ MHz, $(\omega_2 - \omega_b)/2\pi = 14.0$ MHz, $K_1/2\pi = K_2/2\pi = -300.0$ MHz, and $g/2\pi = 2.0$ MHz.

where

$$\begin{aligned} \hat{H}_b &= 4E_{C_b}\hat{n}_b^2 - E_{J_b}\cos(\hat{\varphi}_b) \\ &\approx \omega_b\hat{b}^\dagger\hat{b} + \frac{K_b}{2}\hat{b}^\dagger\hat{b}^2 \end{aligned} \quad (43)$$

is the bus Hamiltonian, which we treat as a weakly nonlinear oscillator of frequency $\omega_b = \sqrt{8E_{C_b}E_{J_b}} - E_{C_b}$ and negative anharmonicity $K_b = -E_{C_b}$. We define the phase operators of the two modes across the snail-like element as $2\hat{\varphi}_\pm = -\hat{\varphi}_b \pm (\hat{\varphi}_r - \varphi_\ell)$, where $\hat{\varphi}_b$ ($\hat{\varphi}_r$) is the phase operator of the bus (resonator) and φ_ℓ is a real-valued scalar determined from the minimization of the potential energy of the circuit. We consider two external flux biases: φ_{s2} in the three-node loop and $\varphi_{sN} - \varphi_{s2}$ in the snail-like circuits. Here, φ_{s2} (φ_{sN}) shifts the cosine potential of the two junctions (N junctions) in the snail-like circuit. Moreover, $\hat{\varphi}_1$ ($\hat{\varphi}_2$) is the phase operator of Q_1 (Q_2). The resonator and bus-resonator Hamiltonians take the form

$$\begin{aligned} \hat{H}_r &= 4E_{C_r}\hat{n}_r^2 - NE_{J_N}\cos\left(\frac{\hat{\varphi}_r - \varphi'_{sN}}{N}\right) + 2\epsilon(t)\hat{n}_r \\ &\quad - 2E_{J_\ell}\cos\left(\frac{\hat{\varphi}_r - \varphi_\ell}{2}\right) - 2E_{J_2}\cos\left(\frac{\hat{\varphi}_r - \varphi'_{s2}}{2}\right), \end{aligned} \quad (44)$$

$$\hat{H}_{br} = -2E_{J_\ell}\left[\cos\left(\frac{3\hat{\varphi}_b}{2}\right) - 1\right]\cos\left(\frac{\hat{\varphi}_r - \varphi_\ell}{2}\right), \quad (45)$$

where $\varphi'_{s2} = \varphi_{s2} + \varphi_\ell$ and $\varphi'_{sN} = \varphi_{sN} + \varphi_\ell$. In these expressions, E_{C_r} is the resonator charging energy, E_{J_ℓ} the

Josephson energy of the symmetrical junctions in the resonator's circuit, E_{J_2} the Josephson energy of each of the two smaller resonator's junctions, and E_{J_N} the Josephson energy of each of the N large junctions in the array. Moreover, $\epsilon(t)$ is the amplitude of the drive of frequency $2(\omega_r - \delta)$ on the resonator, where ω_r is the frequency of the undriven resonator.

Here we aim at stabilizing cat states in the resonator with amplitudes that depend on the bus photon number. Just as in the simplified model discussed in the previous section, transitions between bus states are associated with displacements in the resonator. An advantage of this proposed realization is that the large anharmonicity in the resonator is now determined by the size of the cat state. To this end, we follow Frattini *et al.* [3] by choosing the external fluxes and Josephson energy such as to obtain a cubic nonlinearity of the form $\hat{b}^\dagger\hat{b}(\hat{r}^\dagger + \hat{r})^3$ in \hat{H}_{br} . In the presence of a linear drive on the resonator, the cubic nonlinearity leads to a nearly resonant, bus-photon-number-dependent two-photon drive in the resonator. The Kerr nonlinearity in the resonator can then stabilize bus-photon-number-dependent cat states.

More precisely, we take $E_{J_2} = E_{J_\ell}$, $\varphi_\ell = \pi - 2\zeta$, and $\varphi'_{s2} = -\pi - 2\zeta$, where ζ is a parameter to be defined. With these choices, we have

$$\hat{H}_r = 4E_{C_r}\hat{n}_r^2 - NE_{J_N}\cos\left(\frac{\hat{\varphi}_r - \varphi'_{sN}}{N}\right) + 2\epsilon(t)\hat{n}_r \quad (46)$$

and

$$\hat{H}_{br} \approx \frac{9\pi z_b E_{J_\ell}}{4} (2\hat{b}^\dagger \hat{b} + 1) \times \left[\cos \zeta \sin \left(\frac{\hat{\varphi}_r}{2} \right) + \sin \zeta \cos \left(\frac{\hat{\varphi}_r}{2} \right) \right], \quad (47)$$

where $z_{b(r)} = Z_{b(r)}/R_Q$ is the reduced impedance of the bus (resonator) mode with $R_Q \simeq 6.5 \text{ k}\Omega$ the resistance quantum. In \hat{H}_{br} , the sine and cosine terms that depend on $\hat{\varphi}_r$ are key for implementing the bus-photon-number-dependent cubic nonlinearity $\hat{b}^\dagger \hat{b} (\hat{r}^\dagger + \hat{r})^3$ and the cross-Kerr interaction $\hat{b}^\dagger \hat{b} \hat{r}^\dagger \hat{r}$. Our next step is to apply a displacement transformation $\hat{D}[\xi(t)]$ on the resonator mode to eliminate the drive term that we take to have constant amplitude ϵ_0 for simplicity, $\epsilon(t) = \epsilon_0 \sin[2(\omega_r - \delta)t]$. To achieve this, we take $-i\dot{\xi} + \omega_r \xi + i\epsilon(t)/\sqrt{\pi z_r} = 0$ or, equivalently, $\sqrt{\pi z_r} \dot{\xi}(t) \approx -\Omega \cos[2(\omega_r - \delta)t] + (i\Omega/2) \sin[2(\omega_r - \delta)t]$ with the displacement amplitude $\Omega = 2\epsilon_0/3\omega_r$. By doing so, we obtain the displaced Hamiltonian $\hat{H}^D = \hat{H}_b + \hat{H}_r^D + \hat{H}_{br}^D$ with

$$\hat{H}_r^D \approx \omega_r \hat{r}^\dagger \hat{r} + \frac{K_r}{2} \hat{r}^{\dagger 2} \hat{r}^2 + \frac{\lambda_r}{2} \hat{r}^{\dagger 2} e^{-i2(\omega_r - \delta)t} + \text{H.c.}, \quad (48)$$

$$\hat{H}_{br}^D \approx \chi \left(\hat{b}^\dagger \hat{b} + \frac{1}{2} \right) \hat{r}^\dagger \hat{r} + \frac{\lambda_\ell}{2} (2\hat{b}^\dagger \hat{b} + 1) \hat{r}^{\dagger 2} e^{-i2(\omega_r - \delta)t} + \text{H.c.}, \quad (49)$$

for small φ'_{sN}/N . The above expressions are valid for small reduced mode impedance $\pi z_r \approx \sqrt{2NE_{C_r}/E_{J_N}}$ and assume the rotating-wave approximation. We have introduced the resonator frequency $\omega_r = \sqrt{8E_{C_r}E_{J_N}/N} - E_{C_r}$, the self-Kerr anharmonicity $K_r = -E_{C_r}/N^2$, the two-photon drive amplitude

$$\lambda_r = -\frac{(\pi z_r)^{3/2} \Omega E_{J_N} \varphi'_{sN}}{2N^3}, \quad (50)$$

the cross-Kerr interaction amplitude

$$\chi = -\frac{9\pi z_b \pi z_r E_{J_\ell} \sin(\zeta)}{8}, \quad (51)$$

and the bus-number-dependent two-photon drive amplitude

$$\lambda_\ell = \frac{9\pi z_b (\pi z_r)^{3/2} \Omega E_{J_\ell} \cos(\zeta)}{64}. \quad (52)$$

We, moreover, set $\lambda_r = -2\lambda_\ell$ by a proper choice of the flux biases.

Finally, in a doubly rotating frame at $\omega_r - \delta$ for \hat{r} and at ω_b for \hat{b} , the displaced Hamiltonian \hat{H}^D then approximately becomes

$$\begin{aligned} \hat{H}^D \approx & \frac{K_b}{2} \hat{b}^{\dagger 2} \hat{b}^2 - \frac{K_r \alpha^4}{2} (2\hat{b}^\dagger \hat{b} - 1)^2 \\ & + (\delta + \chi/2 + \chi \hat{b}^\dagger \hat{b}) \hat{r}^\dagger \hat{r} \\ & + \frac{K_r}{2} [\hat{r}^{\dagger 2} + \alpha^2 (2\hat{b}^\dagger \hat{b} - 1)] [\hat{r}^2 + \alpha^2 (2\hat{b}^\dagger \hat{b} - 1)], \end{aligned} \quad (53)$$

where $\alpha^2 = \lambda_\ell/K_r$. Equation (53) is reminiscent of the Kerr-cat Hamiltonian [3,23] with the difference that the amplitude and the orientation of the cat now depend on the bus Fock state number.

The metapotential associated with this Hamiltonian is illustrated in Fig. 7(b). As in Fig. 2 for the simplified system, the different Fock states of the bus mode lead to displaced wells in the I - Q plane. However, because of the combination of the Kerr nonlinearity and the engineered two-photon drive, each Fock state is associated with two metapotential wells [23]. The central idea of blocking the bus-state transition by entangling those states to coherent states in the resonator is, however, unchanged. This is confirmed in Fig. 7(c) that shows $1 - \eta_{1000}$ as a function of the photon number. Apart from additional resonances that can be avoided, the overall behavior is the one expected: we see an exponential reduction of the bus-state hybridization with resonator photon number, as originally predicted by the model of Eq. (2).

Furthermore, it is useful to note that the ac-Stark shift on the bus frequency vanishes in this model, i.e., the ground and first excited states of the bus are both shifted in energy by $K_r \alpha^4/2$. The bus-resonator entanglement is therefore entirely responsible for the exponential suppression observed in Fig. 7(c).

B. Harmonic model with parametric modulation

In Sec. IV we have seen how it is possible to trade the large nonlinear interaction between the bus and the resonator by additional drives. Here, we show how this idea can be realized without modifications to the circuit of Fig. 7. For this second approach, we take $\varphi_\ell = 0$, $\varphi'_{s2} = 2\pi$, $E_{J_2} = \lambda E_{J_\ell}$ with $\lambda = 1 - (3/2)^2 \pi z_b/2$, and $\varphi'_{sN} \bmod 2\pi N = 0$. With these parameter choices, the circuit Hamiltonian can now be written as

$$\hat{H}_b = 4E_{C_b} \hat{n}_b^2 - E_{J_b} \cos(\hat{\varphi}_b) - 2E_{J_\ell} \cos \left(\frac{3\hat{\varphi}_b}{2} \right), \quad (54)$$

$$\hat{H}_r = 4E_{C_r} \hat{n}_r^2 - NE_{J_N} \cos \left(\frac{\hat{\varphi}_r}{N} \right) + 2\epsilon(t) \hat{n}_r, \quad (55)$$

$$\hat{H}_{br} = -2E_{J_\ell} \left[\cos \left(\frac{3\hat{\varphi}_b}{2} \right) - \lambda \right] \left[\cos \left(\frac{\hat{\varphi}_r}{2} \right) - 1 \right]. \quad (56)$$

We note that the reduced mode impedance of the resonator, $\pi z_r \approx \sqrt{2NE_{C_r}/E_{J_N}}$, needs to be made small to prevent the drive on the resonator from resulting in appreciable nonlinear terms due to the cosine potentials and the nearly resonant two-photon and cubic terms. More precisely, we take $1/\sqrt{\pi z_r}$ to be much larger than any displacement in the resonator field associated with the bus Fock states $n \neq 0$, and small compared to $N/\sqrt{\pi z_r}$ for $n = 0$.

As above, we treat the bus and resonator modes as weakly nonlinear oscillators. Importantly, for $n = 0$, we find that $\hat{H}_{br} \approx 0$ and \hat{H}_r is approximately harmonic despite a large displacement in the resonator field. Moreover, for $n \neq 0$, \hat{H}_{br} effectively implements a large cross-Kerr interaction that strongly reduces displacements of the resonator field by rendering the linear drive of the resonator off-resonant. Particularly, we find that

$$\hat{H} \approx \sum_{v=b,r} \left(\omega_v \hat{v}^\dagger \hat{v} + \frac{K_v}{2} \hat{v}^{\dagger 2} \hat{v}^2 \right) + \chi \hat{b}^\dagger \hat{b} \hat{r}^\dagger \hat{r} + i\Omega(t)(\hat{r}^\dagger - \hat{r}). \quad (57)$$

In this expression, we have defined the frequencies $\omega_v \approx \sqrt{8E_{C_v}E_{L_v}} - E_{C_v}$, the reduced mode impedances $\pi z_v \approx \sqrt{2E_{C_v}/E_{L_v}}$, the inductive energies $E_{L_b} = E_{J_b} + 2(3/2)^2 E_{J_\ell}$ and $E_{L_r} = E_{J_N}/N$, the anharmonicities $K_b = -[E_{J_b} + 2(3/2)^4 E_{J_\ell}]E_{C_b}/E_{L_b}$ and $K_r = E_{C_r}/N^2$, and the linear drive amplitude $\Omega(t) = \epsilon(t)/2\sqrt{\pi z_r}$.

We also largely reduce the resonator's anharmonicity K_r by choosing a small E_{C_r} and large N . It is possible with this model to observe the exponential suppression of two-qubit coupling by choosing $\epsilon(t)$ to be nearly resonant with the resonator.

As discussed in Sec. IV, with a reduced anharmonicity in the resonator, an additional drive, which we choose to be of the form

$$\Omega(t) = 2\delta\bar{\alpha}_0 \cos[(\omega_r - \delta)t] + \frac{\omega_m \lambda}{\bar{\alpha}} \sum_{v=\pm} v \sin[(\omega_m + v\omega_r)t], \quad (58)$$

can serve as a complementary mechanism to suppress interactions. In the limits $|\delta/\chi| \ll 1$, $|\chi/\omega_m| \ll 1$, and $|\omega_m/\omega_r| \ll 1$, we find that the bus-state-dependent displacements take the form

$$\alpha_n(t) \approx \frac{\delta\bar{\alpha}_0}{\delta + n\chi} - \frac{i\lambda}{\bar{\alpha}} \cos(\omega_m t), \quad (59)$$

in agreement with Eq. (34). From this point on, the result of Sec. IV follows.

Finally, we emphasize that even though a cross-Kerr type interaction between the bus and the resonator could, in principle, be implemented using a dispersive coupling [28], the dispersive Hamiltonian is invalid at large photon numbers and yields virtual qubit-qubit interactions

through the driven resonator. We also note that a discussion of the leading effects of stray couplings can be found in Appendix D.

VI. CONCLUSION

We have introduced a two-qubit coupler with an exponential on:off ratio, realized by connecting a pair of qubits to a bus mode complemented by a driven ancillary resonator. The cross-Kerr interaction between the bus and the driven resonator results in a displacement of the resonator's field that is conditional on the bus state. Because the displaced resonator states have negligible overlap, bus-state transitions are suppressed exponentially in the amplitude of the drive. In turn, because two-qubit interactions are mediated by bus transitions, the two-qubit coupling results are also strongly suppressed, leading to a high on:off ratio. As a clear demonstration of this mechanism, we have shown how the inverse participation ratio, which is a measure of qubit-bus hybridization, and the spurious cross-Kerr between the qubits are exponentially reduced with the number of photons in the resonator mode. We have also proposed two complementary superconducting quantum circuit implementations of our coupler.

The strong reduction in two-qubit couplings demonstrated here can be advantageous in multiqubit processors, where spectator qubits and long-range qubit-qubit interactions can have detrimental effects [38]. For the same reason, the proposed approach can be particularly useful in all-microwave frequency-fixed qubits architectures with interactions mediated by frequency-fixed buses. Furthermore, our device could be used to improve the performance of a protected-qubit-based processor, where crosstalk could now be exponentially suppressed on demand. The parameter exploration in this work further suggests that exponentially protected qubits, which typically have low transition frequencies and would therefore be naturally closely packed in frequency, would yield a stronger exponential suppression of spurious qubit-qubit interactions.

Finally, we note that possible improvements to the coupler include squeezing the resonator mode to further reduce the overlaps between the resonator states associated with distinct bus states, and extending the ancillary system to multiple modes such that the exponential suppression is now with respect to multiple modes.

ACKNOWLEDGMENTS

We thank Christian K. Andersen, Ross Shillito, and Jens Koch for useful discussions. This work was undertaken in part thanks to funding from NSERC, the Canada First Research Excellence Fund, the Ministère de l'économie et de l'innovation du Québec, and the U.S. Army Research Office under Grant No. W911NF-18-1-0411. This material is based upon work supported by the U.S. Department

of Energy, Office of Science, National Quantum Information Science Research Centers and Quantum Systems Accelerator.

APPENDIX A: POLARON TRANSFORMATION

To gain intuition about the underlying physics of the model, it is useful to move to a frame defined by the time-dependent polaron transformation

$$\hat{P}(t) = e^{-i \int_0^t d\tau [\omega_b + \Delta_{ac}(\tau)] (\hat{b}^\dagger \hat{b} + \sum_j \hat{q}_j^\dagger \hat{q}_j)} e^{-i \omega_d t \hat{r}^\dagger \hat{r}} \times \sum_{n=0}^{\infty} \hat{D}_r[\alpha_n(t)] \otimes |n\rangle\langle n|_b, \quad (\text{A1})$$

where $|n\rangle\langle n|_b$ is the projection operator associated with the eigenstate $|n\rangle$ of the bus mode, and Δ_{ac} is an ac-Stark shift that will be defined below. The displacements $\{\alpha_n(t)\}$ are determined from the damped classical equation of the resonator [cf. Eq. (9)] that result from the bilinear Hamiltonian terms only.

1. Transformed Hamiltonian

Under Eq. (A1), Hamiltonian (2) transforms to $\hat{H}^P = \hat{P}^\dagger \hat{H} \hat{P} - i \hat{P}^\dagger \dot{\hat{P}}$, where

$$\hat{H}^P = \sum_{j=1}^2 \hat{H}_j^P + \hat{H}_{br}^P + \hat{H}_\kappa^P + \hat{H}_g^P, \quad (\text{A2})$$

$$\hat{H}_j^P = (\omega_j - \omega_b - \Delta_{ac}) \hat{q}_j^\dagger \hat{q}_j + \frac{K_j}{2} \hat{q}_j^{\dagger 2} \hat{q}_j^2, \quad (\text{A3})$$

$$\hat{H}_{br}^P = (\delta + \chi \hat{b}^\dagger \hat{b}) \hat{r}^\dagger \hat{r} + \frac{K_b}{2} \hat{b}^{\dagger 2} \hat{b}^2 + \frac{K_r}{2} \hat{r}^{\dagger 2} \hat{r}^2 + \sum_n \Delta_{ac,n} |n\rangle\langle n|_b, \quad (\text{A4})$$

$$\hat{H}_\kappa^P = \frac{i\kappa}{2} \sum_n (\alpha_n \hat{r}^\dagger - \alpha_n^* \hat{r}) |n\rangle\langle n|_b, \quad (\text{A5})$$

$$\hat{H}_g^P = \sum_{j,n} g_j (\hat{q}_j^\dagger e^{i\phi_n} \hat{D}_{n,r} \sqrt{n+1} |n\rangle\langle n+1|_b + \text{H.c.}), \quad (\text{A6})$$

with $i2\phi_n = \alpha_{n+1}^* \alpha_n - \alpha_n^* \alpha_{n+1}$, $\hat{D}_{n,r} = \hat{D}_r(\alpha_{n+1} - \alpha_n)$, $\hat{D}_r(\alpha) = e^{\alpha \hat{r}^\dagger - \alpha^* \hat{r}}$ is the displacement operator in the resonator, and

$$\Delta_{ac,n} = \delta |\alpha_0|^2 - (\delta + n\chi) |\alpha_n|^2 - n \Delta_{ac}, \quad (\text{A7})$$

$$\Delta_{ac} = \delta |\alpha_0|^2 - (\delta + \chi) |\alpha_1|^2. \quad (\text{A8})$$

As we only consider Jaynes-Cummings-type interactions, the transformed Hamiltonian can be reduced to the form

in Eq. (17). In addition, driving the resonator mode introduces an ac-Stark shift $\Delta_{ac}^C(t) = \Delta_1^C(t) - \Delta_0^C(t)$ of the bus frequency given by

$$\Delta_{ac}^C(t) = \delta |\alpha_0(t)|^2 - (\delta + \chi) |\alpha_1(t)|^2. \quad (\text{A9})$$

2. Transformed master equation

The full system dynamics can be described by the Lindblad Master equation formalism

$$\dot{\hat{\rho}} = -i[\hat{H}, \hat{\rho}] + \sum_j \hat{L}_j \hat{\rho} \hat{L}_j^\dagger - \frac{1}{2} \{ \hat{L}_j^\dagger \hat{L}_j, \hat{\rho} \}, \quad (\text{A10})$$

where $\hat{\rho}$ is the density matrix of the system, \hat{H} is the Hamiltonian, and the \hat{L}_j are the collapse operators. Under transformation (A1), the density matrix transforms as $\hat{\rho} = \hat{P} \hat{\rho}^P \hat{P}^\dagger$. It follows that

$$\dot{\hat{\rho}}^P = -i[\hat{H}^P, \hat{\rho}^P] + \sum_j \hat{L}_j^P \hat{\rho}^P \hat{L}_j^{P\dagger} - \frac{1}{2} \{ \hat{L}_j^{P\dagger} \hat{L}_j^P, \hat{\rho}^P \}, \quad (\text{A11})$$

where we have defined the transformed collapse operators $\hat{L}_j^P = \hat{P}^\dagger \hat{L}_j \hat{P}$. As examples, the collapse operators can take the form $\hat{L}_r = \sqrt{\kappa} \hat{r}$, $\hat{L}_{v,\gamma} = \sqrt{\gamma_v} |0\rangle\langle 1|_v$, and $\hat{L}_{v,\varphi} = \sqrt{\gamma_{\varphi,v}/2} (|1\rangle\langle 1|_v - |0\rangle\langle 0|_v)$ for $v = \{b, 1, 2\}$. We find that qubit collapse operators as well as $\hat{L}_{b,\varphi}$ are unchanged under the polaron transformation. However, we have

$$\hat{L}_{b,\gamma}^P = \sqrt{\gamma_b} e^{-i\phi_0} e^{-i \int_0^t d\tau [\omega_b + \Delta_{ac}(\tau)]} \hat{D}_{0,r}^\dagger |0\rangle\langle 1|_b, \quad (\text{A12})$$

$$\hat{L}_r^P = \sqrt{\kappa} \left(\hat{r} + \sum_n \alpha_n |n\rangle\langle n|_b \right). \quad (\text{A13})$$

from where it follows that $\hat{L}_{b,\gamma}^P$ is exponentially suppressed because of the displacement operator in the resonator. Irrespective of this observation, it is worth nothing that $\hat{L}_{b,\gamma}^P$ does not prevent the formation of the polaronic states in the coupler and therefore does not hinder the proposed protocol. In addition, \hat{L}_r^P corresponds to measurement-induced dephasing in the coupler. It is possible to further simplify the master equation within the rotating-wave approximation to

$$\dot{\hat{\rho}}^P = -i[\hat{H}^P - \hat{H}_\kappa^P, \hat{\rho}^P] + \sum_j \hat{L}_j^P \hat{\rho}^P \hat{L}_j^{P\dagger} - \frac{1}{2} \{ \hat{L}_j^{P\dagger} \hat{L}_j^P, \hat{\rho}^P \}, \quad (\text{A14})$$

where $\hat{L}_j^P = \hat{L}_j^P$, except $\hat{L}_r^P = \sqrt{\kappa} \hat{r}$ and we define a new collapse operator $\tilde{\hat{L}}_{b,\gamma\alpha} = \sqrt{\kappa} \sum_n \alpha_n |n\rangle\langle n|_b$ that captures measurement-induced dephasing in the bus.

3. Transitionless driving

Large conditional displacements in the resonator (*off* state) can be prepared by controlling the phase of the envelope in Eq. (10) in time. The same mechanism makes it possible to empty the resonator quickly (*on* state). Imperfections in the envelope lead to deviations in the intended displacements, which we characterize in this section. Using Eq. (9), we find the displacements

$$\alpha_n(t) = i \int_0^t dz \varepsilon(z) e^{i(\delta - i\kappa/2 + n\chi)(z-t)} + \alpha_n(0) e^{-i(\delta - i\kappa/2 + n\chi)t}. \quad (\text{A15})$$

Extending the envelope in Eq. (10) to include both switching-off and switching-on events

$$\begin{aligned} \varepsilon(t) = & \left(\varepsilon_0(t) - \frac{i\dot{\varepsilon}_0(t)}{\delta - i\kappa/2} \right) \Theta(\tau - t) + \varepsilon_0(\tau) \Theta(t - \tau) \Theta(T + \tau - t) \\ & + \left(\varepsilon_0(\tau) - \varepsilon_0(t - T - \tau) + \frac{i\dot{\varepsilon}_0(t - T - \tau)}{\delta - i\kappa/2} \right) \Theta(t - T - \tau) \Theta(T + 2\tau - t), \end{aligned} \quad (\text{A16})$$

where τ is the ramping time to switch off or on the device and T is the time during that the drive is on, we find that

$$\begin{aligned} \alpha_n(t) = & \frac{1}{\delta - i\kappa/2 + n\chi} \begin{cases} 0 & \text{for } t = 0, \\ \varepsilon_0(t) & \text{for } 0 \leq t \leq \tau, \\ \varepsilon_0(\tau) & \text{for } \tau \leq t \leq \tau + T, \\ \varepsilon_0(\tau) - \varepsilon_0(t - \tau - T) & \text{for } \tau + T \leq t \leq 2\tau + T, \\ 0 & \text{for } t \leq 2\tau + T \end{cases} \\ & - \frac{i n \chi}{\delta - i\kappa/2} \left(\int_0^t dz \Theta(\tau - t) - \int_{T+\tau}^t dz \Theta(T + 2\tau - t) \right) \frac{d\varepsilon_0(z)}{dz} \frac{e^{i(\delta - i\kappa/2 + n\chi)(z-t)}}{(-i)(\delta - i\kappa/2 + n\chi)} \\ = & \frac{1}{\delta - i\kappa/2 + n\chi} \begin{cases} 0 & \text{for } t = 0, \\ \varepsilon_0(t) & \text{for } 0 \leq t \leq \tau, \\ \varepsilon_0(\tau) & \text{for } \tau \leq t \leq \tau + T, \\ \varepsilon_0(\tau) - \varepsilon_0(t - \tau - T) & \text{for } \tau + T \leq t \leq 2\tau + T, \\ 0 & \text{for } t \leq 2\tau + T \end{cases} \\ & - \frac{n\chi}{\delta - i\kappa/2} \sum_{k=1}^{\infty} \frac{d^k \varepsilon_0(z)}{dz^k} \frac{e^{i(\delta - i\kappa/2 + n\chi)(z-x)}}{(-i)^k (\delta - i\kappa/2 + n\chi)^{k+1}} \Big|_{z=0}^{z=x} \\ & \times [\delta(t-x)\Theta(\tau-t) - \delta(t-\tau-T-x)\Theta(2\tau+T-t)], \end{aligned} \quad (\text{A17})$$

where we have assumed that $\alpha_n(0) = 0$. It follows that, for

$$\left| \frac{d^k \varepsilon_0(z)}{dz^k} \Big|_{z=0} \right|, \quad \left| \frac{d^k \varepsilon_0(z)}{dz^k} \Big|_{z=\tau} \right| \ll |\delta - i\kappa/2| |\chi|^k, \quad (\text{A18})$$

Eq. (A17) simplifies to Eq. (11) for $\tau \leq t \leq \tau + T$, and vanishes for $t \geq 2\tau + T$. Ultimately, the derivatives of the pulse at the endpoints of the ramp would contribute the most to deviations in the conditional displacements α_n . If one has perfect control over the pulse envelope, the ramping time can be made arbitrarily small, but limitations could arise from pulse imperfections. To see this, we define

the perturbed envelope

$$\varepsilon(t) \rightarrow \varepsilon(t) + \varepsilon_{\text{err}}(t), \quad (\text{A19})$$

where $\varepsilon_{\text{err}}(t)$ is a small time-dependent perturbation. Using integration by parts, we find that

$$\alpha_n(t) \rightarrow \alpha_n(t) + i \sum_{k=0}^{\infty} \frac{d^k \varepsilon_{\text{eff}}(z)}{dz^k} \frac{e^{i(\delta - i\kappa/2 + n\chi)(z-t)}}{(-i)^k (\delta - i\kappa/2 + n\chi)^k} \Big|_0^t. \quad (\text{A20})$$

The effects of nonadiabatic errors are quantified by the ratio between the time derivatives of the drive envelope at

the endpoints and powers of $|\delta - ik/2 + n\chi|$. These errors result in time-dependent fluctuations of $\alpha_n(t)$, which can change the conditional displacements α_n and the ac-Stark shift of the bus. When switching on, TQD errors could result in residual photons in the resonator and ac-Stark shifts in the bus that can affect two-qubit interactions in the *on* state. It is therefore desirable to have a reset scheme for the resonator.

APPENDIX B: NUMERICAL EXPERIMENTS AND ANALYTICAL ESTIMATES

In this section, we provide details regarding the numerical simulations, the derivations for the analytical estimates associated with the inverse participation ratio, and the spurious two-qubit interactions. We also report additional numerical results for the inverse participation ratio and measurement-induced dephasing.

1. Rabi drive experiment

The envelope in Eq. (10) used in Fig. 3 is shown in Fig. 8. The ramping time τ is set to 5 ns independently of $\bar{\alpha}_0$.

2. Inverse participation ratio

In analogy to Fig. 4, the inverse participation ratio for the second qubit, η_{0100} , is computed numerically and reported in Fig. 9. The observations made in Fig. 4 can be extended to Fig. 9. The only difference here is the emergence of a second divergence at small photon numbers for $K_r = 0$. This peak results from the frequency collisions with higher-energy levels in the resonator and the specific choice of parameters. This effect is, however, absent in the presence of anharmonicity in the resonator.

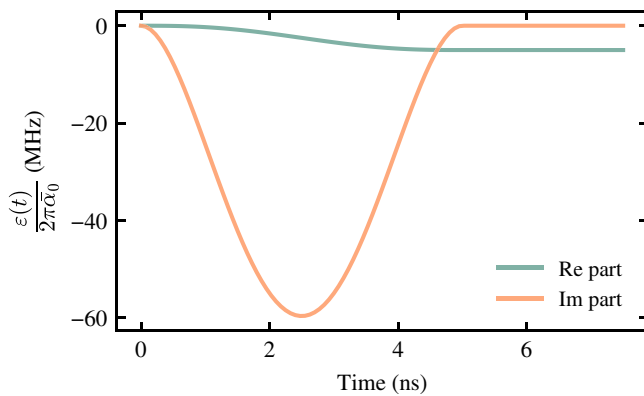


FIG. 8. Envelope $\varepsilon(t)$ in Eq. (10) used for Fig. 3 to turn off the coupler. The drive can be turned off after some arbitrary time in order to turn the coupler back on with the time-reversed pulse shape shown here (cf. Appendix A3).

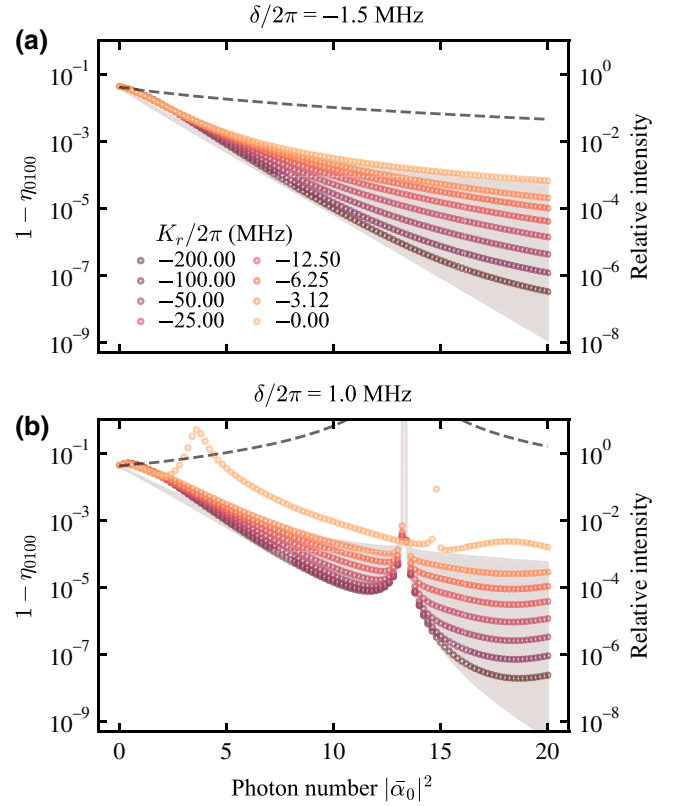


FIG. 9. Suppression of $1 - \eta_{0100}$ with respect to the resonator photon number $|\bar{\alpha}_0|^2$ in the stabilized ground state for (a) $\delta/2\pi = -1.5$ MHz and (b) $\delta/2\pi = 1.0$ MHz. Each data point is computed from numerical diagonalization with a fixed drive amplitude in the resonator. Black lines correspond to the same system but with no drive on the resonator and the bus frequency tuned to the ac-Stark-shifted frequency found in the driven system. The gray regions are bounded by the analytical estimates in Eq. (29) for $K_r \rightarrow \infty$ and $K_r = 0$. We also note the presence of a resonance in (b) for $K_r = 0$ only for a small photon number for this specific choice of system parameters. This results from frequency collisions with higher Fock states in the resonator that can be otherwise prevented by the addition of a resonator anharmonicity. Here $(\omega_1 - \omega_b)/2\pi = 7.0$ MHz, $(\omega_2 - \omega_b)/2\pi = 14.0$ MHz, $K_1/2\pi = K_2/2\pi = -300.0$ MHz, $\chi/2\pi = -20.0$ MHz, and $g/2\pi = 2.0$ MHz.

We now provide an analytical estimate for the inverse participation ratio based on a Schrieffer-Wolff (SW) transformation on Eq. (17), where the Hamiltonian takes the form

$$\hat{H}_I = e^{i \int dt (\hat{H}^P - \hat{H}_k^P)} \hat{H}_g^P e^{-i \int dt (\hat{H}^P - \hat{H}_k^P)}. \quad (\text{B1})$$

To this end, we define the generator

$$\hat{S}_I = i \int dt \hat{H}_I, \quad (\text{B2})$$

under which the Hamiltonian transforms to $\hat{H}_S = e^{\hat{S}_I} \hat{H}_I e^{-\hat{S}_I} + i \dot{\hat{S}}_I = \mathcal{O}(g^2)$. In what follows we describe

different cases where \hat{H}_g^P and $\hat{H}^P - \hat{H}_\kappa^P$ have a particular time dependence used for parametric modulations in Appendix C. Furthermore, we compute the generator back in the polaron frame as

$$\hat{S} = e^{-i \int dt (\hat{H}^P - \hat{H}_\kappa^P)} \hat{S}_I e^{i \int dt (\hat{H}^P - \hat{H}_\kappa^P)}. \quad (\text{B3})$$

This transformation holds for $|\hat{S}| \ll 1$, i.e., if the transition amplitudes are much smaller in magnitude than the energy gaps. Then, the hybridized states are approximately given by $|\psi_{h,v}\rangle = e^{\hat{S}} |\psi_{b,v}\rangle \approx [1 + \hat{S} + \mathcal{O}(g_j^2)] |\psi_{b,v}\rangle$ with $|\psi_{b,v}\rangle$ the bare eigenstates of the full system for $g_j = 0$. An estimation of Eq. (27) using the SW transformation follows as

$$\eta_\mu \approx 1 - 2 \langle \psi_{b,\mu} | \hat{S}^\dagger \hat{S} | \psi_{b,\mu} \rangle. \quad (\text{B4})$$

However, as \hat{S} can be time dependent, it is useful to also define the time-averaged quantity

$$\begin{aligned} \langle \eta_\mu \rangle_t &\approx 1 - 2 \langle \psi_{b,\mu} | \hat{S}^\dagger \hat{S} | \psi_{b,\mu} \rangle_t \\ &= 1 - 2 \lim_{t \rightarrow \infty} \frac{1}{t} \int dt \langle \psi_{b,\mu} | \hat{S}^\dagger \hat{S} | \psi_{b,\mu} \rangle. \end{aligned} \quad (\text{B5})$$

We now identify the generator of the SW transformation for the different cases considered in this manuscript.

a. Static \hat{H}_g^P and $\hat{H}^P - \hat{H}_\kappa^P$

The generator of the SW transformation in this case is

$$\begin{aligned} \hat{S} &= \sum_{j,n,m,k,\ell} \frac{\sqrt{(n+1)(m+1)} \langle k | \hat{D}_{n,r} | \ell \rangle g_j e^{i\phi_n} / \tilde{\Delta}_j}{1 + (mK_j - n\tilde{K}_b) / \tilde{\Delta}_j + q_{j,n,k} - q_{j,n+1,\ell}} \\ &\quad \times |m+1\rangle \langle m|_j |n\rangle \langle n+1|_b |k\rangle \langle \ell|_r - \text{H.c.}, \end{aligned} \quad (\text{B6})$$

$$q_{j,n,k} = \frac{\delta + n\chi}{\tilde{\Delta}_j} k + \frac{K_r}{\tilde{\Delta}_j} \frac{k(k-1)}{2}. \quad (\text{B7})$$

Given that $|\langle k | \hat{D}_{n,r} | \ell \rangle|$ is more strongly suppressed for small Fock state numbers $\{k, \ell\}$, it is clear that the parameters $(\delta + n\chi) / \tilde{\Delta}_j$ and $K_r / \tilde{\Delta}_j$, which control the probability of virtually populating larger Fock states of the resonator, play an important role in the efficiency of the suppression of two-qubit interactions. More precisely, we find that

$$\begin{aligned} \langle \psi_{1000} | \hat{S}^\dagger \hat{S} | \psi_{1000} \rangle &= e^{-|\tilde{\alpha}|^2} \left(\frac{g_j}{\tilde{\Delta}_j} \right)^2 \sum_{\ell=0}^{\infty} \frac{|\tilde{\alpha}|^{2\ell} / \ell!}{(1 - q_{j,1,\ell})^2} \\ &= e^{-|\tilde{\alpha}|^2} \left(\frac{g_1}{\tilde{\Delta}_1} \right)^2 {}_4F_4(\mathbf{p}_1; 1 + \mathbf{p}_1; |\tilde{\alpha}|^2). \end{aligned} \quad (\text{B8})$$

Throughout this work, we consider the two limiting cases $K_r = 0$ and $K_r \rightarrow \infty$. In these limits, it is possible to derive asymptotic expressions for the inverse participation ratio as

$$\eta_{1000}^{|K_r| \rightarrow 0} = 1 - 2 \frac{g_1^2}{\tilde{\Delta}_1^2} e^{-|\tilde{\alpha}|^2} {}_2F_2(\mathbf{q}_1; 1 + \mathbf{q}_1; |\tilde{\alpha}|^2), \quad (\text{B9})$$

$$\eta_{1000}^{|K_r| \rightarrow \infty} = 1 - 2 \frac{g_1^2}{\tilde{\Delta}_1^2} e^{-|\tilde{\alpha}|^2} \left(1 + \frac{|\tilde{\alpha}|^2}{(1 + \zeta_j)^2} \right), \quad (\text{B10})$$

where $\mathbf{q}_j = (1/\zeta_j, 1/\zeta_j)$ and $\zeta_j = -(\delta + \chi) / \tilde{\Delta}_j$. This can be easily generalized to the states 0100 and 1100.

b. Time dependent \hat{H}_g^P and static $\hat{H}^P - \hat{H}_\kappa^P$

We now consider a time-dependent phase

$$e^{i\phi_n} = \sum_{s=-\infty}^{+\infty} \zeta_{n,s} e^{is\omega_m t}, \quad (\text{B11})$$

where ζ_s and ω_m are free time-independent parameters. In this case, the generator takes the form

$$\hat{S} = \sum_{j,n,m,k,\ell,s} \frac{\sqrt{(n+1)(m+1)} \langle k | \hat{D}_{n,r} | \ell \rangle g_j \zeta_{n,s} e^{is\omega_m t} / \tilde{\Delta}_j}{1 + s\omega_m / \tilde{\Delta}_j + (mK_j - n\tilde{K}_b) / \tilde{\Delta}_j + q_{j,n,k} - q_{j,n+1,\ell}} |m+1\rangle \langle m|_j |n\rangle \langle n+1|_b |k\rangle \langle \ell|_r - \text{H.c.} \quad (\text{B12})$$

It then follows that

$$\langle \psi_{1000} | \hat{S}^\dagger \hat{S} | \psi_{1000} \rangle = e^{-|\tilde{\alpha}|^2} \left(\frac{g_j}{\tilde{\Delta}_j} \right)^2 \sum_{\ell, s_1, s_2} \frac{\zeta_{0,s_1} \zeta_{0,s_2}^* e^{i(s_1 - s_2)\omega_m t} |\tilde{\alpha}|^{2\ell} / \ell!}{(1 + s_1\omega_m / \tilde{\Delta}_j - q_{j,1,\ell})(1 + s_2\omega_m / \tilde{\Delta}_j - q_{j,1,\ell})} \quad (\text{B13})$$

with time average

$$\langle \psi_{1000} | \hat{S}^\dagger \hat{S} | \psi_{1000} \rangle_t = e^{-|\tilde{\alpha}|^2} \left(\frac{g_j}{\tilde{\Delta}_j} \right)^2 \sum_{\ell, s} \frac{|\zeta_{0,s}|^2 |\tilde{\alpha}|^{2\ell} / \ell!}{(1 + s\omega_m / \tilde{\Delta}_j - q_{j,1,\ell})^2}. \quad (\text{B14})$$

c. Static \hat{H}_g^P and time dependent $\hat{H}^P - \hat{H}_\kappa^P$

Here we consider a time dependent $\delta \rightarrow \delta - z\omega_m \sin(\omega_m t)$. The generator takes the form

$$\hat{S} = \sum_{j,n,m,k,\ell,s} \frac{\sqrt{(n+1)(m+1)} \langle k | \hat{D}_{n,r} | \ell \rangle g_j e^{i\phi_n} \zeta_{k,\ell,s} e^{i s \omega_m t - i(k-\ell)z \cos(\omega_m t)} / \tilde{\Delta}_j}{1 + s\omega_m / \tilde{\Delta}_j + (mK_j - n\tilde{K}_b) / \tilde{\Delta}_j + q_{j,n,k} - q_{j,n+1,\ell}} |m+1\rangle \langle m|_j |n\rangle \langle n+1|_b |k\rangle \langle \ell|_r - \text{H.c.}, \quad (\text{B15})$$

where the parameters $\zeta_{k,\ell,s}$ are defined with

$$e^{i(k-\ell)z \cos(\omega_m t)} = \sum_{s=-\infty}^{+\infty} i^s J_s[(k-\ell)z] e^{i s \omega_m t} = \sum_{s=-\infty}^{+\infty} \zeta_{k,\ell,s} e^{i s \omega_m t}, \quad (\text{B16})$$

where we have used a Jacobi-Anger expansion. We thus arrive at

$$\langle \psi_{1000} | \hat{S}^\dagger \hat{S} | \psi_{1000} \rangle = e^{-|\bar{\alpha}|^2} \left(\frac{g_j}{\tilde{\Delta}_j} \right)^2 \sum_{\ell,s_1,s_2} \frac{(-1)^{s_1+s_2} J_{s_1}(\ell z) J_{s_2}(\ell z) i^{s_1-s_2} e^{i(s_1-s_2)\omega_m t} |\bar{\alpha}|^{2\ell} / \ell!}{(1 + s_1\omega_m / \tilde{\Delta}_j - q_{j,1,\ell})(1 + s_2\omega_m / \tilde{\Delta}_j - q_{j,1,\ell})} \quad (\text{B17})$$

and the time-averaged version

$$\langle \psi_{1000} | \hat{S}^\dagger \hat{S} | \psi_{1000} \rangle_t = e^{-|\bar{\alpha}|^2} \left(\frac{g_j}{\tilde{\Delta}_j} \right)^2 \sum_{\ell,s} \frac{J_s^2(\ell z) |\bar{\alpha}|^{2\ell} / \ell!}{(1 + s\omega_m / \tilde{\Delta}_j - q_{j,1,\ell})^2}. \quad (\text{B18})$$

d. Time dependent \hat{H}_g^P and $\hat{H}^P - \hat{H}_\kappa^P$

Finally, we combine the two previous cases, namely we consider a time-dependent phase

$$e^{i\phi_n} = \sum_{s=-\infty}^{+\infty} \zeta_{n,s}^\phi e^{i s \omega_m^\phi t} \quad (\text{B19})$$

and a time dependent $\delta \rightarrow \delta - z\omega_m^\delta \sin(\omega_m^\delta t)$ with

$$e^{i(k-\ell)z \cos(\omega_m^\delta t)} = \sum_{s=-\infty}^{+\infty} i^s J_s[(k-\ell)z] e^{i s \omega_m^\delta t} = \sum_{s=-\infty}^{+\infty} \zeta_{k,\ell,s}^\delta e^{i s \omega_m^\delta t}. \quad (\text{B20})$$

The generator takes the form

$$\hat{S} = \sum_{j,n,m,k,\ell,s,r} \frac{\sqrt{(n+1)(m+1)} \langle k | \hat{D}_{n,r} | \ell \rangle g_j \zeta_{n,s}^\phi \zeta_{k,\ell,r}^\delta e^{i(s\omega_m^\phi + r\omega_m^\delta)t - i(k-\ell)z \cos(\omega_m^\delta t)} / \tilde{\Delta}_j}{1 + (s\omega_m^\phi + r\omega_m^\delta) / \tilde{\Delta}_j + (mK_j - n\tilde{K}_b) / \tilde{\Delta}_j + q_{j,n,k} - q_{j,n+1,\ell}} |m+1\rangle \langle m|_j |n\rangle \langle n+1|_b |k\rangle \langle \ell|_r - \text{H.c.} \quad (\text{B21})$$

With this we find that

$$\begin{aligned} \langle \psi_{1000} | \hat{S}^\dagger \hat{S} | \psi_{1000} \rangle &= e^{-|\bar{\alpha}|^2} \left(\frac{g_j}{\tilde{\Delta}_j} \right)^2 \sum_{\ell,s_1,s_2,r_1,r_2} i^{s_1-s_2+r_1-r_2} e^{i(s_1-s_2)\omega_m^\phi t + i(r_1-r_2)\omega_m^\delta t} \\ &\times \frac{(-1)^{r_1+r_2} \zeta_{0,s_1} \zeta_{0,s_2}^* J_{r_1}(\ell z) J_{r_2}(\ell z) |\bar{\alpha}|^{2\ell} / \ell!}{[1 + (s_1\omega_m^\phi + r_1\omega_m^\delta) / \tilde{\Delta}_j - q_{j,1,\ell}][1 + (s_2\omega_m^\phi + r_2\omega_m^\delta) / \tilde{\Delta}_j - q_{j,1,\ell}]}, \end{aligned} \quad (\text{B22})$$

which, under time averaging, reduces to

$$\langle \psi_{1000} | \hat{S}^\dagger \hat{S} | \psi_{1000} \rangle_t = e^{-|\bar{\alpha}|^2} \left(\frac{g_j}{\tilde{\Delta}_j} \right)^2 \sum_{\ell,s,r} \frac{|\zeta_{0,s}|^2 J_r^2(\ell z) |\bar{\alpha}|^{2\ell} / \ell!}{[1 + (s\omega_m^\phi + r\omega_m^\delta) / \tilde{\Delta}_j - q_{j,1,\ell}]^2}. \quad (\text{B23})$$

Here we have assumed that $s\omega_m^\phi + r\omega_m^\delta = 0$ only for $s = 0$ and $r = 0$.

3. Sweeping through frequency collisions

To understand the impact of frequency collisions between the qubits and the bus as the photon number in the resonator is increased, it is useful to consider the toy-model Hamiltonian $\hat{H}_\vartheta(t) = \vartheta e^{i \int_0^t dt' \Delta_\vartheta(t')} \hat{q}_1^\dagger \hat{b} + \text{H.c.}$ between Q_1 and the bus in the interaction picture, where we ignore Q_2 for simplicity. Here, $\Delta_\vartheta(t)$ as defined in Eq. (24) is the instantaneous detuning between these systems including ac-Stark shifts, and ϑ is an effective coupling strength. To simplify the discussion, we focus on the case where $\Delta_\vartheta = \Delta_1 - \delta \nu t$ with Δ_1 the initial detuning between Q_1 and the bus, $\delta = \omega_r - \omega_d$ as before, and the rate $\nu = |\dot{\bar{\alpha}}_0(t_f)|^2 / t_f$ is set to a constant, where t_f is the final time.

Assuming that $\delta \nu / \Delta_1 > 0$ such that there is a crossing at some time $\tau = \Delta_1 / \delta \nu$, an excitation in Q_1 leaks to B with probability $1 - e^{-2\pi|\vartheta|^2/|\delta|\nu}$, i.e., the Landau-Zener formula [40,41]. A fast sweep $\nu \gg 2\pi|\vartheta|^2/|\delta|$ naturally minimizes leakage to the bus.

Given that $\bar{\alpha}_0(t) = \varepsilon_0(t)/\delta$ in our TQD protocol (cf. Appendix A), the envelope is therefore $\varepsilon_0(t) = \delta\sqrt{\nu}t$. It follows that $d^k \varepsilon_0(t)/dt^k = (1/2)^{(k)} \nu^k \varepsilon_0(t) / \bar{\alpha}_0^{2k}(t)$ must be much smaller in magnitude than χ^{k+1} to prevent nonadiabatic errors in the TQD protocol for $k \geq 1$ (cf. Appendix A). In other words, $|2\chi^2 \bar{\alpha}_0(t)/\delta| \gg \nu \gg \pi|\vartheta|^2/|\delta|$. Here we emphasize that ϑ is an effective coupling strength between Q_1 and B near the resonance,

which we expect to be exponentially suppressed with $\vartheta \sim g_1 e^{-|\bar{\alpha}_0(t)|^2/2}$.

Finally, setting $\nu = \eta 2\chi^2 |\bar{\alpha}_0/\delta|$, where $0 < \eta < 1$ (with $\eta = 1$ corresponding to the upper bound defined above), we estimate the leakage probability to be of the order of

$$P \sim 1 - \exp[-\eta^{-1} \pi |\bar{\alpha}_0(\tau)|^{-1} e^{-|\bar{\alpha}_0(\tau)|^2} |g_1/\chi|^2], \quad (\text{B24})$$

where $\bar{\alpha}_0(\tau)$ is the coherent state amplitude at the crossing at time $t = \tau$. For $\eta \sim 1.0$, $|g_1/\chi| \sim 0.2$, we find that $P \sim 0.001$ for $|\bar{\alpha}_0(\tau)| \sim 2.0$ and $P \sim 5 \times 10^{-6}$ for $|\bar{\alpha}_0(\tau)| \sim 3.0$. We can further suppress P for even larger $|\bar{\alpha}_0(\tau)|$ and smaller $|g_1/\chi|$. Note that, for smaller sweeping rates, it is possible to further reduce to the leakage probability by dynamically decoupling the bus using, for example, a flux modulation of the bus frequency [42] that is compatible with our scheme. In the presence of this modulation, only processes that do not conserve the bus excitation number are exponentially suppressed.

4. Two-qubit interactions

In this section we demonstrate how the matrix elements of the displacement operator in \hat{H}_g^P [cf. Eq. (17)] yields exponentially suppressed two-qubit interactions by deriving an upper bound based on the inverse participation ratio. Consider the time-evolution operator in the interaction picture

$$\hat{U}_I(t) = \mathcal{T} e^{-i \int_0^t d\tau \hat{H}_I(\tau)} = \sum_{n=0}^{\infty} \frac{(-i)^n}{n!} \int_0^t d\tau_1 \cdots \int_0^t d\tau_n \mathcal{T} \hat{H}_I(\tau_1) \cdots \hat{H}_I(\tau_n), \quad (\text{B25})$$

where \mathcal{T} is the time-ordering operator and we have used the interaction picture Hamiltonian defined in Eq. (B1). It is convenient to approximate Eq. (B25) using a Magnus expansion,

$$\hat{U}_I = e^{-i \int_0^t d\tau \hat{H}_I^M(\tau)}, \quad (\text{B26})$$

where \hat{H}_I^M is an effective Hamiltonian. Up to fourth order in g_j we have

$$\begin{aligned} \hat{H}_I^M(t) &\approx \hat{H}_I(t) - \frac{1}{2} [\hat{H}_I(t), \hat{S}_I(t)] + \frac{i}{6} \int_0^t d\tau_1 \{ [\hat{H}_I(t), \hat{H}_I(\tau_1) \hat{S}_I(\tau_1)] + [\hat{S}_I(\tau_1) [\hat{H}_I(\tau_1), \hat{H}_I(t)]] \} \\ &+ \frac{1}{12} \int_0^t \int_0^{\tau_1} d\tau_1 d\tau_2 \{ [\hat{H}_I(t) \hat{H}_I(\tau_1) \hat{H}_I(\tau_2), \hat{S}_I(\tau_2)] + [\hat{H}_I(t), \hat{H}_I(\tau_1) \hat{H}_I(\tau_2) \hat{S}_I(\tau_2)] \} \\ &+ \frac{1}{12} \int_0^t \int_0^{\tau_1} d\tau_1 d\tau_2 \{ [\hat{H}_I(t), \hat{H}_I(\tau_1) \hat{H}_I(\tau_2) \hat{S}_I(\tau_2)] + [\hat{H}_I(\tau_1), \hat{H}_I(\tau_2) \hat{S}_I(\tau_2) \hat{H}_I(t)] \}, \end{aligned} \quad (\text{B27})$$

where, based on Eq. (B2), we have introduced $\hat{S}_I(t) = i \int_0^t d\tau \hat{H}_I(\tau)$.

To compute effective two-qubit interactions, we project \hat{H}_I^M in the ground state of the coupler, valid in the dispersive coupling limit. Because of the form of \hat{H}_I [cf. Eq. (B1)], only terms of even order in g_j remain in \hat{H}_I^M . Defining the projection operator $\hat{P} = |0_b, 0_r\rangle\langle 0_b, 0_r|$, we compute the effective two-qubit Hamiltonian

$$\hat{H}_I^{q-q}(t) = \text{Tr}_c[\hat{H}_I^M(t)\hat{P}], \quad (\text{B28})$$

corresponding to \hat{H}_I^M , where the coupler mode is traced out assuming that it is stabilized in its ground state. For compactness, we define $\hat{H}_I^M = \sum_{n=1}^4 \hat{H}_{I,n}^M$, where $\hat{H}_{I,n}^M$ incorporates the couplings g_j at n th order. In what follows we approximate the qubits and coupler as two-level systems. This approximation is valid in the limit where the qubit-coupler detunings are small compared to the anharmonicities of the qubits and the coupler. Our results can, however, be extended to include the effects of finite anharmonicity. We therefore write

$$\hat{H}_I(t) \approx \sum_{j,k,\ell} g_j e^{i\tilde{\Delta}_j(1+q_{j,0,k}-q_{j,1,\ell})t} \hat{A}_{k,\ell} \hat{\sigma}_{+j} + \text{H.c.}, \quad (\text{B29})$$

$$\hat{A}_{k,\ell} = e^{i\phi_0} \langle k|\hat{D}_{0,r}|\ell\rangle |k\rangle\langle \ell|_r \hat{\sigma}_{-b}, \quad (\text{B30})$$

$$q_{j,n,k} = \frac{\delta + n\chi}{\tilde{\Delta}_j} k + \frac{K_r}{\tilde{\Delta}_j} \frac{k(k-1)}{2} = \frac{r_{n,k}}{\tilde{\Delta}_j}, \quad (\text{B31})$$

where $\hat{\sigma}_{-j}$ ($\hat{\sigma}_{-b}$) is the spin ladder operator, the two-level approximation of \hat{q}_j (\hat{b}). The interaction picture generator \hat{S}_I and the polaron frame generator \hat{S} then take the form

$$\hat{S}_I(t) \approx \sum_{j,k,\ell} \frac{g_j}{\tilde{\Delta}_j} e^{i\tilde{\Delta}_j(1+q_{j,0,k}-q_{j,1,\ell})t} \frac{\hat{A}_{k,\ell} \hat{\sigma}_{+j}}{1 + q_{j,0,k} - q_{j,1,\ell}} - \text{H.c.}, \quad (\text{B32})$$

$$\hat{S} \approx \sum_{j,k,\ell} \frac{g_j}{\tilde{\Delta}_j} \frac{\hat{A}_{k,\ell} \hat{\sigma}_{+j}}{1 + q_{j,0,k} - q_{j,1,\ell}} - \text{H.c.}, \quad (\text{B33})$$

in analogy to Eqs. (B2) and (B3). Our goal is to find an upper bound on the amplitude of two-qubit interactions in Eq. (B28) corresponding to a partial trace over Eq. (B27). This upper bound can be obtained from the Cauchy-Schwartz inequality,

$$|\text{Tr}(\hat{A}\hat{B})| \leq \sqrt{\text{Tr}(\hat{A}^\dagger \hat{A})} \sqrt{\text{Tr}(\hat{B}^\dagger \hat{B})} = |\hat{A}|_F |\hat{B}|_F, \quad (\text{B34})$$

where $|\cdot|_F$ stands for the Frobenius norm. We separate the two-qubit interactions by the order in the coupling strengths g_j and stop at fourth order. However, the following analysis can be extended to higher orders in the coupling strengths.

a. Second-order interactions

We now focus on the two-qubit interactions of second order in the coupling strengths in Eq. (B28). To this end, it is convenient to expand

$$\text{Tr}[\hat{H}_{I,2}^M(t)\hat{P}] = -\frac{1}{2} \text{Tr}_c[\hat{H}_I(t)\hat{S}_I(t)\hat{P}] + \text{H.c.}, \quad (\text{B35})$$

where

$$\begin{aligned} \text{Tr}_c[\hat{H}_I(t)\hat{S}_I(t)\hat{P}] &= \sum_{s_1, s_2=1}^2 e^{i(\tilde{\Delta}_{qs_1} - \tilde{\Delta}_{qs_2})t} g_{s_1} \text{Tr} \\ &\times \left(\sum_{\ell=0}^{\infty} \hat{A}_{0,\ell} \frac{g_{s_2}}{\tilde{\Delta}_{qs_2}} \frac{\hat{A}_{0,\ell}^\dagger}{1 - q_{s_2,1,\ell}} \hat{P} \right) \\ &\times \hat{\sigma}_{+s_1} \hat{\sigma}_{-s_2}. \end{aligned} \quad (\text{B36})$$

Interestingly, applying Eq. (B34) yields

$$\begin{aligned} &\left| \text{Tr} \left(\sum_{\ell=0}^{\infty} \hat{A}_{0,\ell} \frac{g_{s_2}}{\tilde{\Delta}_{qs_2}} \frac{\hat{A}_{0,\ell}^\dagger}{1 - q_{s_2,1,\ell}} \hat{P} \right) \right| \\ &\leq \left\| \sum_{\ell=0}^{\infty} \hat{A}_{0,\ell} \right\|_F \left\| \sum_{\ell=0}^{\infty} \frac{g_{s_2}}{\tilde{\Delta}_{qs_2}} \frac{\hat{A}_{0,\ell}^\dagger}{1 - q_{s_2,1,\ell}} \hat{P} \right\|_F, \end{aligned} \quad (\text{B37})$$

where

$$\left\| \sum_{\ell=0}^{\infty} \hat{A}_{0,\ell} \right\|_F = \|\lvert 0\rangle\langle 0|_r e^{i\phi_0} \hat{D}_{0,r}|_F \lvert \hat{\sigma}_{-b}\rangle|_F = 1. \quad (\text{B38})$$

Furthermore,

$$\begin{aligned} &\left\| \sum_{\ell=0}^{\infty} \frac{g_{s_2}}{\tilde{\Delta}_{qs_2}} \frac{\hat{A}_{0,\ell}^\dagger}{1 - q_{s_2,1,\ell}} \hat{P} \right\|_F \\ &= \sqrt{\left(\frac{g_{s_2}}{\tilde{\Delta}_{qs_2}} \right)^2 \sum_{\ell=0}^{\infty} \frac{|\langle \ell|\hat{D}_{0,r}|0\rangle|^2}{(1 - q_{s_2,1,\ell})^2}} \\ &\approx \sqrt{\frac{1 - \eta_{\Omega(s_2)}}{2}} \end{aligned} \quad (\text{B39})$$

with $\Omega(s_2) = 1000$ for $s_2 = 1$ and 0100 for $s_2 = 2$, and where we have used the dispersive limit expression for $1 - \eta_\mu$ [cf. Eq. (B8)]. Since each term in Eq. (B35) is bounded in magnitude by $\max_{v \in \{1000, 0100\}} \sqrt{1 - \eta_v}$, it follows that Eq. (B35) is equally bounded in magnitude by $\max_{v \in \{1000, 0100\}} \sqrt{1 - \eta_v}$. Intuitively, this means that the virtual interaction is always smaller in magnitude than $|g_j g_j / \tilde{\Delta}_j|$.

b. Fourth-order interactions

We now demonstrate that the $\max_{v \in \{1000, 0100\}} \sqrt{1 - \eta_v}$ bound holds for higher-order two-qubit interactions. First, we expand the commutators such that

$$\begin{aligned} \text{Tr}_c(\hat{H}_{I,4}^M \hat{P}) &= \frac{1}{12} \int_0^t \int_0^{\tau_1} d\tau_1 d\tau_2 (2 \text{Tr}_c[\hat{H}_I(t) \hat{H}_I(\tau_1) \hat{H}_I(\tau_2) \hat{S}_I(\tau_2) \hat{P}] - \text{Tr}_c\{[\hat{H}_I(\tau_1), \hat{H}_I(t)] \hat{H}_I(\tau_2) \hat{S}_I(\tau_2) \hat{P}\} \\ &\quad - \text{Tr}_c\{[\hat{H}_I(\tau_2), \hat{H}_I(t)] \hat{H}_I(\tau_1) \hat{S}_I(\tau_2) \hat{P}\} - \text{Tr}_c\{[\hat{H}_I(\tau_1), \hat{H}_I(\tau_2)] \hat{H}_I(t) \hat{S}_I(\tau_2) \hat{P}\} \\ &\quad - \text{Tr}_c\{[\hat{H}_I(t), \hat{H}_I(\tau_1)] \hat{S}_I(\tau_2) \hat{H}_I(\tau_2) \hat{P}\} - \text{Tr}_c\{[\hat{H}_I(t), \hat{H}_I(\tau_2)] \hat{S}_I(\tau_2) \hat{H}_I(\tau_1) \hat{P}\} \\ &\quad - \text{Tr}_c\{[\hat{H}_I(\tau_1), \hat{H}_I(\tau_2)] \hat{S}_I(\tau_2) \hat{H}_I(t) \hat{P}\}) + \text{H.c.} \end{aligned} \quad (\text{B40})$$

Second, we find that

$$\begin{aligned} \text{Tr}_c[\hat{H}_I(t_1) \hat{H}_I(t_2) \hat{H}_I(t_3) \hat{S}_I(t_4) \hat{P}] &= \sum_{s_1, \dots, s_4=1}^2 e^{i\tilde{\Delta}_{q_{s_1}} t_1} e^{-i\tilde{\Delta}_{q_{s_2}} t_2} e^{i\tilde{\Delta}_{q_{s_3}} t_3} e^{-i\tilde{\Delta}_{q_{s_4}} t_4} g_{s_1} g_{s_2} g_{s_3} \\ &\quad \times \text{Tr} \left(\sum_{k, \ell, m=0}^{\infty} e^{-ir_{1,k}(t_1-t_2) - ir_{0,\ell}(t_2-t_3) - ir_{1,m}(t_3-t_4)} \hat{A}_{0,k} \hat{A}_{\ell,k}^\dagger \hat{A}_{\ell,m} \frac{g_{s_4}}{\tilde{\Delta}_{q_{s_4}}} \frac{\hat{A}_{0,m}^\dagger}{1 - q_{s_4,1,m}} \hat{P} \right) \\ &\quad \times \hat{\sigma}_{+,s_1} \hat{\sigma}_{-,s_2} \hat{\sigma}_{+,s_3} \hat{\sigma}_{-,s_4} \end{aligned} \quad (\text{B41})$$

and, similarly,

$$\begin{aligned} \text{Tr}_c[\hat{H}_I(t_1) \hat{H}_I(t_2) \hat{S}_I(t_3) \hat{H}_I(t_4) \hat{P}] &= - \sum_{s_1, \dots, s_4=1}^2 e^{i\tilde{\Delta}_{q_{s_1}} t_1} e^{-i\tilde{\Delta}_{q_{s_2}} t_2} e^{i\tilde{\Delta}_{q_{s_3}} t_3} e^{-i\tilde{\Delta}_{q_{s_4}} t_4} g_{s_1} g_{s_2} g_{s_4} \\ &\quad \times \text{Tr} \left(\sum_{k, \ell, m=0}^{\infty} e^{-ir_{1,k}(t_1-t_2) - ir_{0,\ell}(t_2-t_3) - ir_{1,m}(t_3-t_4)} \hat{A}_{0,k} \hat{A}_{\ell,k}^\dagger \frac{g_{s_3}}{\tilde{\Delta}_{q_{s_3}}} \frac{\hat{A}_{\ell,m} \hat{A}_{0,m}^\dagger}{1 + q_{s_3,0,\ell} - q_{s_3,1,m}} \hat{P} \right) \\ &\quad \times \hat{\sigma}_{+,s_1} \hat{\sigma}_{-,s_2} \hat{\sigma}_{+,s_3} \hat{\sigma}_{-,s_4}. \end{aligned} \quad (\text{B42})$$

As was done in the previous section, we apply Eq. (B34) to find an upper bound on Eq. (B41):

$$\begin{aligned} &\left| \text{Tr} \left(\sum_{k, \ell, m=0}^{\infty} e^{-ir_{1,k}(t_1-t_2) - ir_{0,\ell}(t_2-t_3) - ir_{1,m}(t_3-t_4)} \hat{A}_{0,k} \hat{A}_{\ell,k}^\dagger \hat{A}_{\ell,m} \frac{g_{s_4}}{\tilde{\Delta}_{q_{s_4}}} \frac{\hat{A}_{0,m}^\dagger}{1 - q_{s_4,1,m}} \hat{P} \right) \right| \\ &\leq \left\| \sum_{k, \ell, m=0}^{\infty} e^{-ir_{1,k}(t_1-t_2) - ir_{0,\ell}(t_2-t_3) - ir_{1,m}(t_3-t_4)} \hat{A}_{0,k} \hat{A}_{\ell,k}^\dagger \hat{A}_{\ell,m} \right\|_F \left\| \sum_{m=0}^{\infty} \frac{g_{s_4}}{\tilde{\Delta}_{q_{s_4}}} \frac{\hat{A}_{0,m}^\dagger}{1 - q_{s_4,1,m}} \hat{P} \right\|_F \\ &\leq \left\| \sum_{k, \ell, m=0}^{\infty} \hat{A}_{0,k} \hat{A}_{\ell,k}^\dagger \hat{A}_{\ell,m} \right\|_F \left\| \sum_{m=0}^{\infty} \frac{g_{s_4}}{\tilde{\Delta}_{q_{s_4}}} \frac{\hat{A}_{0,m}^\dagger}{1 - q_{s_4,1,m}} \hat{P} \right\|_F, \end{aligned} \quad (\text{B43})$$

Here it can also be verified that $|\sum_{k, \ell, m=0}^{\infty} \hat{A}_{0,k} \hat{A}_{\ell,k}^\dagger \hat{A}_{\ell,m}|_F = 1$ and where

$$\left\| \sum_{m=0}^{\infty} \frac{g_{s_4}}{\tilde{\Delta}_{q_{s_4}}} \frac{\hat{A}_{0,m}^\dagger}{1 - q_{s_4,1,m}} \hat{P} \right\|_F \approx \sqrt{\frac{1 - \eta_{\Omega(s_4)}}{2}}. \quad (\text{B44})$$

Similarly, Eq. (B34) can be applied on Eq. (B42):

$$\begin{aligned} & \left| \text{Tr} \left(\sum_{k,\ell,m=0}^{\infty} e^{-ir_{1,k}(t_1-t_2)-ir_{0,\ell}(t_2-t_3)-ir_{1,m}(t_3-t_4)} \hat{A}_{0,k} \hat{A}_{\ell,k}^\dagger \frac{g_{s_3}}{\tilde{\Delta}_{q_{s_3}}} \frac{\hat{A}_{\ell,m} \hat{A}_{0,m}^\dagger}{1+q_{s_3,0,\ell}-q_{s_3,1,m}} \hat{P} \right) \right| \\ & \leq \left\| \sum_{k,\ell=0}^{\infty} e^{-ir_{1,k}(t_1-t_2)-ir_{0,\ell}(t_2-t_3)} \hat{A}_{0,k} \hat{A}_{\ell,k}^\dagger \right\|_F \left\| \sum_{\ell,m=0}^{\infty} e^{-ir_{1,m}(t_3-t_4)} \frac{g_{s_3}}{\tilde{\Delta}_{q_{s_3}}} \frac{\hat{A}_{\ell,m} \hat{A}_{0,m}^\dagger}{1+q_{s_3,0,\ell}-q_{s_3,1,m}} \hat{P} \right\|_F \\ & \leq \left\| \sum_{k,\ell=0}^{\infty} \hat{A}_{0,k} \hat{A}_{\ell,k}^\dagger \right\|_F \left\| \sum_{\ell,m=0}^{\infty} \frac{g_{s_3}}{\tilde{\Delta}_{q_{s_3}}} \frac{\hat{A}_{\ell,m} \hat{A}_{0,m}^\dagger}{1+q_{s_3,0,\ell}-q_{s_3,1,m}} \hat{P} \right\|_F, \end{aligned} \quad (\text{B45})$$

where $|\sum_{k,\ell=0}^{\infty} \hat{A}_{0,k} \hat{A}_{\ell,k}^\dagger|_F = 1$ and

$$\left\| \sum_{\ell,m=0}^{\infty} \frac{g_{s_3}}{\tilde{\Delta}_{q_{s_3}}} \frac{\hat{A}_{\ell,m} \hat{A}_{0,m}^\dagger}{1+q_{s_3,0,\ell}-q_{s_3,1,m}} \hat{P} \right\|_F = \sqrt{\sum_{\ell,m,m'=0}^{\infty} \left(\frac{g_{s_3}}{\tilde{\Delta}_{q_{s_3}}} \right)^2 \frac{\langle 0|\hat{D}_{0,r}|m'\rangle \langle m'|\hat{D}_{0,r}^\dagger|\ell\rangle \langle \ell|\hat{D}_{0,r}|m\rangle \langle m|\hat{D}_{0,r}^\dagger|0\rangle}{(1+q_{s_3,0,\ell}-q_{s_3,1,m})(1+q_{s_3,0,\ell}-q_{s_3,1,m})}}. \quad (\text{B46})$$

Considering this norm to be bounded from above by the limiting cases $\delta = 0$ and $K_r = 0$, we find that

$$\left\| \sum_{\ell,m=0}^{\infty} \frac{g_{s_3}}{\tilde{\Delta}_{q_{s_3}}} \frac{\hat{A}_{\ell,m} \hat{A}_{0,m}^\dagger}{1+q_{s_3,0,\ell}-q_{s_3,1,m}} \hat{P} \right\|_F \lesssim \sqrt{\sum_{\ell,m=0}^{\infty} \left(\frac{g_{s_3}}{\tilde{\Delta}_{q_{s_3}}} \right)^2 \frac{|\langle m|\hat{D}_{0,r}|0\rangle|^2}{(1-q_{s_3,1,m})^2}} \approx \sqrt{\frac{1-\eta_{\Omega(s_3)}}{2}}. \quad (\text{B47})$$

As previously found for second-order interactions, all contributions are bounded in magnitude by $\max_{v \in \{1000,0100\}} \sqrt{1-\eta_v}$. These observations can be straightforwardly extended to higher orders in a similar fashion.

This implies that exponentially suppressing $1-\eta_\mu$ will equally exponentially suppress virtual two-qubit interactions. However, we stress that this only provides an estimate for the order of magnitude.

5. Measurement-induced dephasing

In order to quantify the dephasing induced by the coupler drive, we express Eq. (26) in the hybridized eigenbasis

$$\hat{L}_b^P = \sqrt{\frac{\kappa|\bar{\alpha}|^2}{4}} \sum_{v,v'} c_{v,v'} |\psi_{h,v}\rangle \langle \psi_{h,v'}| \quad (\text{B48})$$

with

$$c_{v,v'} = \langle \psi_{h,v} | (|1\rangle\langle 1|_b - |0\rangle\langle 0|_b) | \psi_{h,v'} \rangle. \quad (\text{B49})$$

To study the effects of bus dephasing on Q_1 alone, we first trace out Q_2, B , and R in the hybridized basis where all three have zero excitation

$$\hat{L}_1^P \approx \sum_{ij} \langle \psi_{h,i000} | \hat{L}_b^P | \psi_{h,j000} \rangle | \psi_{h,i000} \rangle \langle \psi_{h,j000} |. \quad (\text{B50})$$

We then apply a rotating-wave approximation to obtain

$$\hat{L}_1^P \approx \sqrt{\frac{\kappa|\bar{\alpha}|^2}{4}} \sum_i c_{i000;i000} |\psi_{h,i000}\rangle \langle \psi_{h,i000}|. \quad (\text{B51})$$

Because the total excitation number in Q_1, Q_2 , and B is conserved under Eq. (17) and the interaction in Eq. (17) dominantly yields hybridization between 1 and B , we neglect $\langle \psi_{h,1000} | \psi_{b,010k} \rangle \approx 0$. We also use the fact that $\sum_k |\langle \psi_{h,0000} | \psi_{b,000k} \rangle|^2 = 1$ due to total excitation number conservation, and, finally, $\sum_k |\langle \psi_{h,1000} | \psi_{b,100k} \rangle|^2 \approx 1 - \sum_k |\langle \psi_{h,1000} | \psi_{b,001k} \rangle|^2$. It follows that $c_{1000;1000} \approx 2 \sum_k |\langle \psi_{h,1000} | \psi_{b,001k} \rangle|^2 - 1$ and $c_{0000;0000} \approx -1$, leading to

$$\begin{aligned} \hat{L}_1^P & \approx \sqrt{\frac{\kappa|\bar{\alpha}|^2}{4}} \sum_{k=0}^{\infty} |\langle \psi_{h,1000} | \psi_{b,001k} \rangle|^2 (|\psi_{h,1000}\rangle \langle \psi_{h,1000}| \\ & - |\psi_{h,0000}\rangle \langle \psi_{h,0000}|). \end{aligned} \quad (\text{B52})$$

The dephasing rate of Q_1 can be estimated by computing the dephasing rate associated with Eq. (B52), which takes the form

$$\begin{aligned} \gamma_{\varphi,1} & = \frac{\kappa|\bar{\alpha}|^2}{2} \left(\sum_{k=0}^{\infty} |\langle \psi_{h,1000} | \psi_{b,001k} \rangle|^2 \right)^2 \\ & \approx \frac{\kappa|\bar{\alpha}|^2}{2} \frac{1-\eta_{1000}}{2}, \end{aligned} \quad (\text{B53})$$

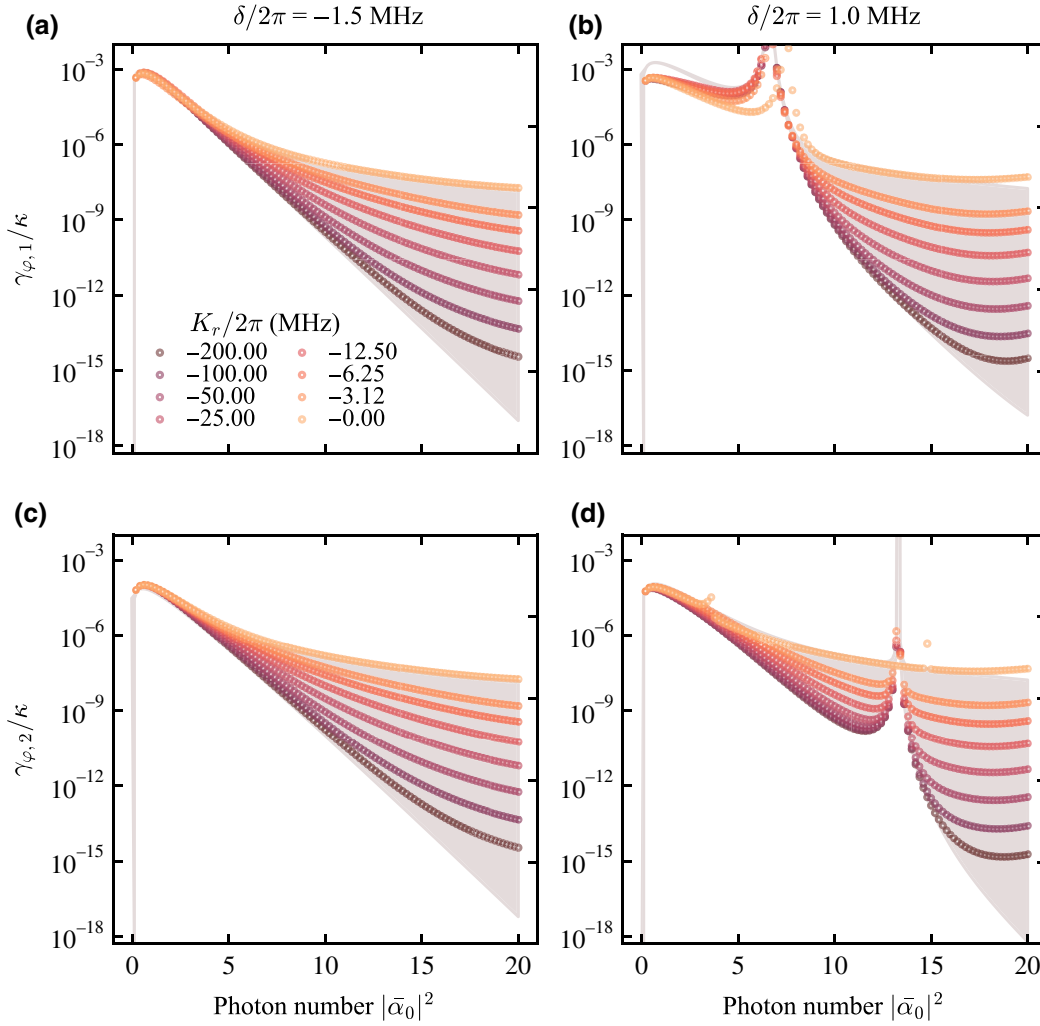


FIG. 10. Measurement-induced dephasing rates in qubits 1 and 2. Dephasing rate for (a),(b) qubit 1, and (c),(d) qubit 2. The gray regions correspond to the analytical estimates in Eq. (32) with Eqs. (B9) and (B10). The $\delta/2\pi = -1.5$ MHz (a),(c) and $\delta/2\pi = 1.0$ MHz (b),(d) correspond to two different parameter regimes set by the sign of δ . Here $(\omega_1 - \omega_b)/2\pi = 7.0$ MHz, $(\omega_2 - \omega_b)/2\pi = 14.0$ MHz, $K_1/2\pi = K_2/2\pi = -300.0$ MHz, $\chi/2\pi = -20.0$ MHz, $g/2\pi = 2.0$ MHz, and $\kappa/2\pi = 100.0$ kHz.

where the second line follows from the Schrieffer-Wolff transformation [cf. Eq. (B4)]. The expression above is obtained under a rotating-wave approximation, which is valid for $|\gamma_{\varphi,1}/\tilde{\Delta}_1| \ll 1$. An expression for the second qubit is obtained by simply replacing the subscript 1000 by 0100. Measurement-induced dephasing rates in the qubits are estimated numerically from diagonalization and are reported in Fig. 10.

6. Parameter regimes

We have seen in Figs. 4 and 5 that the choice of frequency detuning between the resonator and the drive δ , which controls the sign of the ac-Stark shift between the qubits and the bus, has both a quantitative and qualitative impact on the system. To better understand this behavior, we consider again Eqs. (28) and (29) where we now

express the generalized hypergeometric functions as

$${}_4F_4(\mathbf{p}_j, 1 + \mathbf{p}_j; |\bar{\alpha}|^2) = \sum_{n=0}^{\infty} \frac{|\bar{\alpha}|^{2n}}{n!} \prod_{k=\pm} \left(1 + \frac{n}{p_{jk}}\right)^{-2}. \quad (\text{B54})$$

We recall that in this expression $p_{j\pm} = \beta[1 \pm \sqrt{1 + 2\tilde{\Delta}_j\beta^{-2}/K_r}]$ with $\beta = (\delta + \chi)/K_r - 1/2$ and where $\tilde{\Delta}_j$ is the ac-Stark-shifted detuning given in Eq. (24). Physically, Eq. (B54) corresponds to a weighted sum over all virtual transitions to higher-energy levels in the resonator for a displacement $\bar{\alpha}$ during a $0 \rightarrow 1$ transition in the bus. The poles $1 + n/p_{jk}$ in Eq. (B54) correspond to frequency collisions with these higher-energy levels.

Given that we wish to maximize the exponential suppression of $1 - \eta_\mu$ [i.e., the exponential factor in Eqs. (28)

and (29)], we want ${}_4F_4(\mathbf{p}_j, 1 + \mathbf{p}_j; |\bar{\alpha}|^2)$ to be as close as possible to unity. To have a monotonic suppression with respect to $|\bar{\alpha}|^2$, this parameter should be chosen such as to avoid frequency collisions corresponding to the poles of Eq. (B54). With these constraints, we define two key parameter regimes below. In what follows we take $(\kappa/2)^2 \ll |\delta(\delta + \chi)|$, but we note that κ also plays a role in controlling the ac-Stark shift of the bus and can be seen as an additional knob. To simplify the analysis below, it is useful to note that, for $K_r = 0$, we find that $p_{j+} \rightarrow \infty$ and $p_{j-} \rightarrow -\tilde{\Delta}_j/(\delta + \chi)$, while for $|K_r| \gg \{|\tilde{\Delta}_j|, |\delta + \chi|\}$, we find that $p_{j+} \rightarrow -1 + 2(\delta + \chi - \tilde{\Delta}_j)/K_r$ and $p_{j-} \rightarrow 2\tilde{\Delta}_j/K_r$.

a. Monotonic suppression

We first focus on the situation illustrated in panels (a) of Figs. 4 and 5 where there are no frequency collisions between the different modes of the system and the suppression factor is a smooth function of the photon number. There are two possible sources of frequency collisions: (i) the ac-Stark-shifted qubit-bus detuning $\tilde{\Delta}_j$ of Eq. (24) and (ii) higher-energy levels in the resonator as captured by Eq. (B54).

First, to avoid a collision where $\tilde{\Delta}_j = 0$, the ac-Stark-shifted qubit-bus detuning should ideally grow in magnitude with respect to $\bar{\alpha}$. This, in turn, implies that $\omega_{qj} - \omega_b$ and $\delta(\delta + \chi)/\chi \approx \delta$ should have opposite signs. Considering the second source of frequency collisions, $p_{j\pm} > 0$ in Eq. (B54) suppresses frequency collisions with higher-energy levels in the resonator. For $K_r = 0$, this condition is achieved with $p_{j-} = -\tilde{\Delta}_j/(\delta + \chi) > 0$, meaning that $\tilde{\Delta}_j$ and $\delta + \chi$ have opposite signs. Combining this with the above finding, it follows that δ and χ have the same signs, and opposite signs to $\omega_{qj} - \omega_b$. We stress that this choice of parameters is equally compatible with the large- $|K_r|$ limit because $|1/p_{j-}|$ is then large.

Combining the above with the fact that $|\delta/\chi| \ll 1$ for large conditional displacements allows us to define the parameter regime for monotonic suppression of $1 - \eta_\mu$ as

$$|\delta/\chi| \ll 1, \quad (\omega_j - \omega_b)\delta < 0, \quad (\omega_j - \omega_b)\chi < 0. \quad (\text{B55})$$

Because the nonlinearity of Josephson junctions is negative, in panels (a) of Figs. 4 and 5 we choose $\chi < 0$ and $\omega_j - \omega_b > 0$.

b. Nonmonotonic and strong suppression

As illustrated in panels (b) of Figs. 4 and 5, working in a parameter regime where the behavior of $1 - \eta_\mu$ with the photon number is nonmonotonic can lead to stronger suppression. A first observation to understanding this effect is that, taking $p_{j-} \propto \tilde{\Delta}_j$ and $p_{j-} \rightarrow 0$, forces Eq. (B54)

to be unity. Moreover, we can exploit the fact that symmetric two-qubit interactions, such as the ZZ interaction, are suppressed when the bus frequency lies between the qubit frequencies. As a result, the choice $\tilde{\Delta}_1 + \tilde{\Delta}_2 = 0$ minimizes the ZZ interaction in Eq. (31) in the limit of large anharmonicities with respect to the detunings, i.e., $|\tilde{\Delta}_j/K_j| \ll 1$ and $|\tilde{\Delta}_j/\tilde{K}_b| \ll 1$.

Based on these arguments, we define a second parameter regime according to

$$|\delta/\chi| \ll 1, \quad (\omega_j - \omega_b)\delta > 0, \quad (\omega_j - \omega_b)\chi < 0. \quad (\text{B56})$$

The essential difference with respect to Eq. (B55) is that δ has now changed sign. In this regime, the ac-Stark shift of the bus mode changes the sign of the qubit-bus detunings for some $\bar{\alpha}$, something that can help suppress spurious interactions.

It is worth highlighting that the protocol presented here works best for small qubit-bus detunings $|\tilde{\Delta}_j|$ relative to $|\chi|$. This is because the drive on the resonator, close to its resonance frequency, renders the energy gaps between the stabilized states in the resonator smaller in magnitude than in the bare energy spectrum of the resonator. Without anharmonicity in the resonator, these energy gaps are predominantly set by $|\chi|$.

Finally, although we have focused on $\bar{\alpha}_0$ with the TQD protocol, one could have chosen to grow $\bar{\alpha}_1$ for example, such as to still suppress the dominant $0 \leftrightarrow 1$ transition in the bus. The main reason for the focus on $\bar{\alpha}_0$ is that, in this case, δ is made small but $\delta + \chi$ is large, thus preventing transitions to higher-energy states of the resonator.

APPENDIX C: EFFECTIVE PARAMETRIC MODULATION

In this section we provide supporting analytical derivations and numerical results for the parametric modulation (PAM) scheme presented in Sec. IV and discuss another decoupling scheme based on a longitudinal drive (LD) in the resonator to mimic the effects of an anharmonicity. We also show that the two schemes can be potentially combined to offer stronger suppression of qubit-qubit interactions.

1. PAM: additional tones in the resonator drive

We comment on the effects of the fast-oscillating contributions in Eq. (40). As previously stated, these terms impose a lower bound on the time averaged $1 - \eta_\mu$. For large ω_m as compared to δ and χ , this lower bound is approximately $2(g/\omega_m)^2$. In the particular case of $\omega_m = \omega_0|\bar{\alpha}|$, such that the voltage drive amplitude in the resonator is displacement independent, we observe that the asymptotic behavior in the suppression is polynomial in $|\bar{\alpha}|$. We also stress that an appreciable anharmonicity K_r

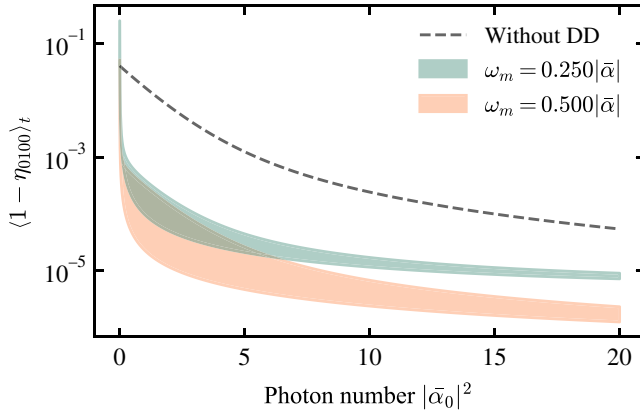


FIG. 11. Dynamical decoupling in the bus: time-averaged inverse participation ratio against photon number in the ground state. Here we assume two additional tones $\omega_r \pm \omega_m$ with amplitude $\omega_m \lambda / \bar{\alpha}$, and we choose ω_m such that the voltage-drive amplitude is fixed for all $\bar{\alpha}$. The regions are bounded by $\lambda = \lambda_0$, where $J_0(\lambda_0) = 0$, and a $\pm 10\%$ error on λ_0 . Note that we exclude anharmonicity in the resonator ($K_r = 0$). The parameters are $\delta/2\pi = -1.0$ MHz, $\chi/2\pi = -20.0$ MHz, $(\omega_1 - \omega_b)/2\pi = 7.0$ MHz, $(\omega_2 - \omega_b)/2\pi = 14.0$ MHz, $K_1/2\pi = K_2/2\pi = -300.0$ MHz, and $g/2\pi = 2.0$ MHz.

in the resonator could in principle result in additional frequency collisions due to negative $s\omega_m/\tilde{\Delta}_1$, where s is an integer. Finally, and in addition to Fig. 6, we report the inverse participation of the second qubit in Fig. 11. For both Figs. 6 and 11, we plot the time-averaged inverse participation ratio obtained in Appendix B2b.

2. LD: longitudinal drive in the resonator

We now discuss how a longitudinal drive in the resonator can help recover a strong suppression in the absence

of large anharmonicity and without the need for fine tuning. Our starting point is Eq. (B18). In the $z \rightarrow \infty$ limit, the asymptotic behavior of the Bessel functions is

$$J_\nu(z) \sim \sqrt{\frac{2}{\pi z}} \cos\left(z - \frac{2\nu + 1}{4}\pi\right), \quad (\text{C1})$$

and we also have $J_\nu(-z) = (-1)^\nu J_\nu(z)$. It follows that the matrix elements of Eq. (B15) are renormalized by $|(k - \ell)z|^{-1/2}$ for $k \neq \ell$. This result is appealing given that the suppression of two-qubit interactions is strongest if the resonator is constrained to Fock states of small photon number and it is desirable to suppress $0 \rightarrow k$ transitions in the resonator, as shown in Fig. 12.

A key advantage of this scheme is that it might be possible to relax parameter constraints for $\tilde{\Delta}_q$ and χ due to the simulated anharmonicity. Regarding the physical implementation, it can range from a modulated detuning in the voltage drive to flux modulating a superconducting loop with junctions. The results shown in Fig. 12 correspond to the time-averaged participation ratio obtained in Appendix B2c.

3. PAM and LD in parallel

A key challenge in combining PAM and LD is to prevent frequency collisions. Having simultaneously large modulation frequencies for both schemes is therefore not a good option. Given that the lower bound on $1 - \eta_\mu$ is dominantly set by the modulation frequency in PAM, we choose this frequency to be the largest. Since the modulation frequency in LD is small, we can choose z to be large. We indeed observe in Fig. 13 that it is possible to grow stronger suppression factors by increasing z . Figure 13 illustrates the time-averaged inverse participation obtained in Appendix D.

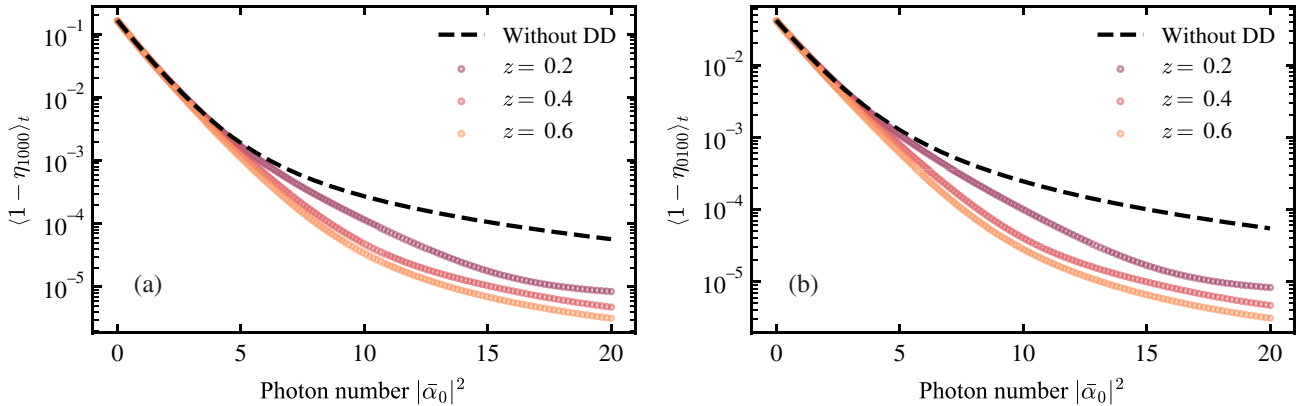


FIG. 12. Dynamical decoupling in the resonator: time-averaged inverse participation ratio against photon number in the ground state for the states (a) 1000 and (b) 0100. We assume an additional longitudinal drive $\delta \rightarrow \delta - z\omega_m \sin(\omega_m t)$ in the resonator with $\omega_m = 1.0$ GHz. Note that no anharmonicity is considered for the resonator ($K_r = 0$). The parameters are $\delta/2\pi = -1.0$ MHz, $\chi/2\pi = -20.0$ MHz, $(\omega_1 - \omega_b)/2\pi = 7.0$ MHz, $(\omega_2 - \omega_b)/2\pi = 14.0$ MHz, $K_1/2\pi = K_2/2\pi = -300.0$ MHz, and $g/2\pi = 2.0$ MHz.

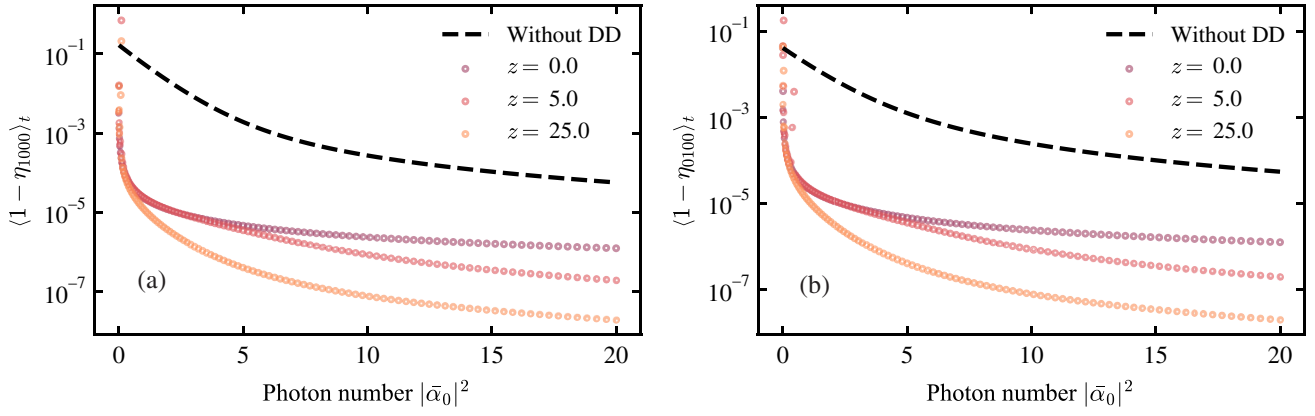


FIG. 13. Dynamical decoupling in the bus and in the resonator: time-averaged inverse participation ratio against photon number in the ground state for the states (a) 1000 and (b) 0100. Here we assume two additional tones $\omega_r \pm \omega_m^\phi$ in the voltage drive with amplitude $\omega_m^\phi \lambda / \bar{\alpha}$, and we choose $\omega_m^\phi = 0.5\bar{\alpha}$ such that the voltage-drive amplitude is fixed for all $\bar{\alpha}$ with $\lambda = \lambda_0$, where $J_0(\lambda_0) = 0$. We assume an additional longitudinal drive $\delta \rightarrow \delta - z\omega_m^\delta \sin(\omega_m^\delta t)$ in the resonator with $\omega_m^\delta = 10.0$ MHz. The parameters are $\delta/2\pi = -1.0$ MHz, $\chi/2\pi = -20.0$ MHz, $(\omega_1 - \omega_b)/2\pi = 7.0$ MHz, $(\omega_2 - \omega_b)/2\pi = 14.0$ MHz, $K_1/2\pi = K_2/2\pi = -300.0$ MHz, and $g/2\pi = 2.0$ MHz.

APPENDIX D: SUPERCONDUCTING IMPLEMENTATION

The inverse participation ratio for the second qubit is illustrated in Fig. 14 and should be contrasted to that of panel (c) in Fig. 7.

We conclude with a remark on stray couplings, not captured by Eq. (2), but most likely present in a superconducting circuit implementation. For instance, direct coupling g_{1-2} between the qubits cannot be suppressed by manipulating the coupler and, in that case, η_μ includes an additional term $-2g_{1-2}^2/(\omega_1 - \omega_2)^2$ that bounds $1 - \eta_\mu$. However, this bound can be conveniently lowered by detuning the qubits and improving circuit design

such that g_{1-2} is minimized. It is also worth noting that this interaction is typically very small compared to desired couplings. Another possibility for the presence of stray couplings is to have spurious qubit-resonator interactions. In this case, virtual two-qubit transitions mediated by the resonator are not exponentially suppressed. However, if the resonator is far detuned in frequency with respect to the qubits, these interactions can be greatly reduced. Finally, stray dispersive coupling between the bus and the resonator can also exist. However, this type of nonidealities are not particularly detrimental, as the resulting weak hybridization between the bus and the resonator does not prevent the suppression of two-qubit interactions.

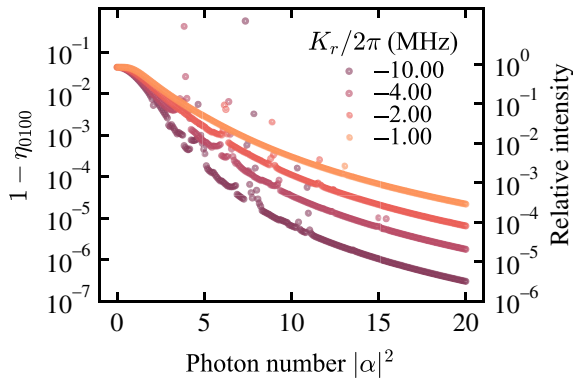


FIG. 14. The quantity $1 - \eta_{0100}$ estimated with the numerical diagonalization of the full system with the effective Hamiltonian in Eq. (53) with $\delta/2\pi = 19.9$ MHz, $\chi/2\pi = -20.0$ MHz [parameter regime of Fig. 7(c), where $|\alpha_0| \rightarrow 0$]. Here $(\omega_1 - \omega_b)/2\pi = 7.0$ MHz, $(\omega_2 - \omega_b)/2\pi = 14.0$ MHz, $K_1/2\pi = K_2/2\pi = -300.0$ MHz, and $g/2\pi = 2.0$ MHz.

- [1] A. O. Niskanen, K. Harrabi, F. Yoshihara, Y. Nakamura, S. Lloyd, and J. S. Tsai, Quantum coherent tunable coupling of superconducting qubits, *Science* **316**, 723 (2007).
- [2] J. Majer, J. M. Chow, J. M. Gambetta, Jens Koch, B. R. Johnson, J. A. Schreier, L. Frunzio, D. I. Schuster, A. A. Houck, A. Wallraff, A. Blais, M. H. Devoret, S. M. Girvin, and R. J. Schoelkopf, ‘Coupling superconducting qubits via a cavity bus, *Nature* **449**, 443 EP – (2007).
- [3] N. E. Frattini, U. Vool, S. Shankar, A. Narla, K. M. Sliwa, and M. H. Devoret, 3-wave mixing josephson dipole element, *Appl. Phys. Lett.* **110**, 222603 (2017).
- [4] Fei Yan, Philip Krantz, Youngkyu Sung, Morten Kjaergaard, Daniel L. Campbell, Terry P. Orlando, Simon Gustavsson, and William D. Oliver, Tunable Coupling Scheme for Implementing High-Fidelity Two-Qubit Gates, *Phys. Rev. Appl.* **10**, 054062 (2018).
- [5] Eyob A. Sete, Angela Q. Chen, Riccardo Manenti, Shobhan Kulshreshtha, and Stefano Poletto, Floating Tunable Coupler for Scalable Quantum Computing Architectures, *Phys. Rev. Appl.* **15**, 064063 (2021).

- [6] A. D. K. Finck, S. Carnevale, D. Klaus, C. Scerbo, J. Blair, T. G. McConkey, C. Kurter, A. Carniol, G. Keefe, M. Kumph, and O. E. Dial, Suppressed crosstalk between two-junction superconducting qubits with mode-selective exchange coupling, [arXiv:2105.11495 \[quant-ph\]](#) (2021).
- [7] L. Casparis, N. J. Pearson, A. Kringhøj, T. W. Larsen, F. Kuemmeth, J. Nygård, P. Krogstrup, K. D. Petersson, and C. M. Marcus, Voltage-controlled superconducting quantum bus, *Phys. Rev. B* **99**, 085434 (2019).
- [8] E. Christiane and Maria Homann, Experiments on two-resonator circuit quantum electrodynamics: A superconducting quantum switch, (2013).
- [9] Yu Chen *et al.*, Qubit Architecture with High Coherence and Fast Tunable Coupling, *Phys. Rev. Lett.* **113**, 220502 (2014).
- [10] Frank Arute, Kunal Arya, Ryan Babbush, Dave Bacon, Joseph C. Bardin, Rami Barends, Rupak Biswas, Sergio Boixo, Fernando GSL Brandao, and David A. Buell *et al.*, Quantum supremacy using a programmable superconducting processor, *Nature* **574**, 505 (2019).
- [11] David C. McKay, Stefan Filipp, Antonio Mezzacapo, Easwar Magesan, Jerry M. Chow, and Jay M. Gambetta, Universal Gate for Fixed-Frequency Qubits via a Tunable bus, *Phys. Rev. Appl.* **6**, 064007 (2016).
- [12] Marco Roth, Marc Ganzhorn, Nikolaj Moll, Stefan Filipp, Gian Salis, and Sebastian Schmidt, Analysis of a parametrically driven exchange-type gate and a two-photon excitation gate between superconducting qubits, *Phys. Rev. A* **96**, 062323 (2017).
- [13] Ji kun Xie, Sheng li Ma, Zhi peng Yang, and Zhen Li, Fu li Li, Quantum switch for coupling highly detuned superconducting qubits, *Phys. Lett. A* **382**, 2626 (2018).
- [14] M. Kounalakis, C. Dickel, A. Bruno, N. K. Langford, and G. A. Steele, Tuneable hopping and nonlinear cross-kerr interactions in a high-coherence superconducting circuit, *Npj Quantum Inf.* **4**, 38 (2018).
- [15] Ji Chu and Fei Yan, Coupler-Assisted Controlled-Phase Gate with Enhanced Adiabaticity, *Phys. Rev. Appl.* **16**, 054020 (2021).
- [16] Michele C. Collodo, Johannes Herrmann, Nathan Lacroix, Christian Kraglund Andersen, Ants Remm, Stefania Lazar, Jean-Claude Besse, Theo Walter, Andreas Wallraff, and Christopher Eichler, Implementation of Conditional Phase Gates Based on Tunable zz Interactions, *Phys. Rev. Lett.* **125**, 240502 (2020).
- [17] Youngkyu Sung, Leon Ding, Jochen Braumüller, Antti Vepsäläinen, Bharath Kannan, Morten Kjaergaard, Ami Greene, Gabriel O. Samach, Chris McNally, David Kim, Alexander Melville, Bethany M. Niedzielski, Mollie E. Schwartz, Jonilyn L. Yoder, Terry P. Orlando, Simon Gustavsson, and William D. Oliver, Realization of High-Fidelity cz and zz -Free Iswap Gates with a Tunable Coupler, *Phys. Rev. X* **11**, 021058 (2021).
- [18] Eyob A. Sete, Nicolas Didier, Angela Q. Chen, Shobhan Kulshreshtha, Riccardo Manenti, and Stefano Poletto, Parametric-Resonance Entangling Gates with a Tunable Coupler, *Phys. Rev. Appl.* **16**, 024050 (2021).
- [19] Peter Groszkowski, Austin G. Fowler, Felix Motzoi, and Frank K. Wilhelm, Tunable coupling between three qubits as a building block for a superconducting quantum computer, *Phys. Rev. B* **84**, 144516 (2011).
- [20] Pranav Mundada, Gengyan Zhang, Thomas Hazard, and Andrew Houck, Suppression of Qubit Crosstalk in a Tunable Coupling Superconducting Circuit, *Phys. Rev. Appl.* **12**, 054023 (2019).
- [21] Jaseung Ku, Xuexin Xu, Markus Brink, David C. McKay, Jared B. Hertzberg, Mohammad H. Ansari, and B. L. T. Plourde, Suppression of Unwanted zz Interactions in a Hybrid Two-Qubit System, *Phys. Rev. Lett.* **125**, 200504 (2020).
- [22] Peng Zhao, Peng Xu, Dong Lan, Ji Chu, Xinsheng Tan, Haifeng Yu, and Yang Yu, High-Contrast zz Interaction Using Superconducting Qubits with Opposite-Sign Anharmonicity, *Phys. Rev. Lett.* **125**, 200503 (2020).
- [23] Shruti Puri, Samuel Boutin, and Alexandre Blais, Engineering the quantum states of light in a kerr-nonlinear resonator by two-photon driving, *Npj Quantum Inf.* **3**, 18 (2017).
- [24] A. Grimm, N. E. Frattini, S. Puri, S. O. Mundhada, S. Touzard, M. Mirrahimi, S. M. Girvin, S. Shankar, and M. H. Devoret, Stabilization and operation of a kerr-cat qubit, *Nature* **584**, 205 (2020).
- [25] Vladimir E. Manucharyan, Jens Koch, Leonid I. Glazman, and Michel H. Devoret, Fluxonium: Single cooper-pair circuit free of charge offsets, *Science* **326**, 113 (2009).
- [26] Long B. Nguyen, Yen-Hsiang Lin, Aaron Somoroff, Raymond Mencia, Nicholas Grabon, and Vladimir E. Manucharyan, High-Coherence Fluxonium Qubit, *Phys. Rev. X* **9**, 041041 (2019).
- [27] Alexandre Blais, Ren-Shou Huang, Andreas Wallraff, S. M. Girvin, and R. J. Schoelkopf, Cavity quantum electrodynamics for superconducting electrical circuits: An architecture for quantum computation, *Phys. Rev. A* **69**, 062320 (2004).
- [28] Alexandre Blais, Arne L. Grimsmo, S. M. Girvin, and Andreas Wallraff, Circuit quantum electrodynamics, *Rev. Mod. Phys.* **93**, 025005 (2021).
- [29] Andrew J. Kerman, Quantum information processing using quasiclassical electromagnetic interactions between qubits and electrical resonators, *New J. Phys.* **15**, 123011 (2013).
- [30] P.-M. Billangeon, J. S. Tsai, and Y. Nakamura, Circuit-qed-based scalable architectures for quantum information processing with superconducting qubits, *Phys. Rev. B* **91**, 094517 (2015).
- [31] Nicolas Didier, Jérôme Bourassa, and Alexandre Blais, Fast Quantum Non-Demolition Readout from Longitudinal Qubit-Oscillator Interaction, *Phys. Rev. Lett.* **115**, 203601 (2015).
- [32] Dmitry A. Ryndyk, Pino D'Amico, Gianarelio Cuniberti, and Klaus Richter, Charge-memory polaron effect in molecular junctions, *Phys. Rev. B* **78**, 085409 (2008).
- [33] P. T. Cochrane, G. J. Milburn, and W. J. Munro, Macroscopically distinct quantum-superposition states as a bosonic code for amplitude damping, *Phys. Rev. A* **59**, 2631 (1999).
- [34] Mazyar Mirrahimi, Zaki Leghtas, Victor V. Albert, Steven Touzard, Robert J. Schoelkopf, Liang Jiang, and Michel H. Devoret, Dynamically protected cat-qubits: A new paradigm for universal quantum computation, *New J. Phys.* **16**, 045014 (2014).

- [35] Jens Koch, Terri M. Yu, Jay Gambetta, A. A. Houck, D. I. Schuster, J. Majer, Alexandre Blais, M. H. Devoret, S. M. Girvin, and R. J. Schoelkopf, Charge-insensitive qubit design derived from the cooper pair box, *Phys. Rev. A* **76**, 042319 (2007).
- [36] Michael Victor Berry, Transitionless quantum driving, *J. Phys. A: Math. Theor.* **42**, 365303 (2009).
- [37] J. Gambetta, A. Blais, D. I. Schuster, A. Wallraff, L. Frunzio, J. Majer, M. H. Devoret, S. M. Girvin, and R. J. Schoelkopf, Qubit-photon interactions in a cavity: Measurement-induced dephasing and number splitting, *Phys. Rev. A* **74**, 042318 (2006).
- [38] Christoph Berke, Evangelos Varvelis, Simon Trebst, Alexander Altland, and David P. DiVincenzo, Transmon platform for quantum computing challenged by chaotic fluctuations, [arXiv:2012.05923](https://arxiv.org/abs/2012.05923) [quant-ph] (2020).
- [39] Ferdinand Evers and Alexander D. Mirlin, Anderson transitions, *Rev. Mod. Phys.* **80**, 1355 (2008).
- [40] Milena Grifoni and Peter Hänggi, Driven quantum tunneling, *Phys. Rep.* **304**, 229 (1998).
- [41] Le Tuan Anh Ho and Liviu F. Chibotaru, A simple derivation of the landau–zener formula, *Phys. Chem. Chem. Phys.* **16**, 6942 (2014).
- [42] Yulin Wu, Li-Ping Yang, Ming Gong, Yarui Zheng, Hui Deng, Zhiguang Yan, Yanjun Zhao, Keqiang Huang, Anthony D. Castellano, William J. Munro, Kae Nemoto, Dong-Ning Zheng, C. P. Sun, Yu-xi Liu, Xiaobo Zhu, and Li Lu, An efficient and compact switch for quantum circuits, *Npj Quantum Inf.* **4**, 50 (2018).